Citation: Rodríguez-Pintó, A., Serra-Kiel, J., Bernaola, G., Barnolas, A., Pueyo, E.L., Tosquella, J., Arbués, P., Scholger, R., 2022. The early/middle Eocene transition at the Ésera valley (South-Central Pyrenees): Implications in Shallow Benthic Zones (SBZ). Geologica Acta, 20.6, 1-25.
DOI: 10.1344/GeologicaActa2022.20.6

geologica acta

The early/middle Eocene transition at the Ésera valley (South-Central Pyrenees): Implications in Shallow Benthic Zones (SBZ)

A. Rodríguez-Pintó[1] J. Serra-Kiel[2+] G. Bernaola[3] A. Barnolas[4*] E.L. Pueyo[5, 6] J. Tosquella[7] P. Arbués[2, 8] R. Scholger[9]

[1]Freelance Geologist consultant
E-mail: adrianaropi14@gmail.com

[2]Universitat de Barcelona, Facultat de Ciències de la Terra, Departament de Dinàmica de la Terra i de l'Oceà
Carrer de Martí Franquès s/n, 08028 Barcelona, Spain

[3]Department of Mining-Metallurgy Engineering and Material Science, Faculty of Engineering in Bilbao, University of the Basque Country (UPV/EHU)
Plaza Ingeniero Torres Quevedo 1, Bilbao, Spain. E-mail: gilen.bernaola@ehu.eus

[4]Instituto Geológico y Minero de España (CSIC)
Ríos Rosas 23, 28003-Madrid, Spain. E-Mail: toni.barnolas@gmail.com

[5]Instituto Geológico y Minero de España (CSIC)
Unidad de Zaragoza. C/M. Lasala 44, 9ºB, 50006, Zaragoza, Spain. E-mail: unaim@igme.es

[6]Unidad Asociada en Ciencias de la Tierra IGME(CSIC)/Universidad de Zaragoza

[7]Departamento de Ciencias de la Tierra, Facultad de Ciencias Experimentales, Universidad de Huelva
Campus del Carmen, Avenida de las Fuerzas Armadas s/n, 21071 Huelva, Spain. E-mail: josep@uhu.es

[8]Geomodels Research Institute, University of Barcelona
Carrer de Martí Franquès s/n, 08028 Barcelona, Spain

[9]Chair of Applied Geophysics, University of Leoben
Franz Josef-Straße 18, 8700 Leoben, Àustria

*Corresponding author
+ Deceased

ABSTRACT

An integrated study including magnetostratigraphy, larger benthic foraminifera and calcareous nannofossil biostratigraphy is presented herein. This work was performed in shallow marine siliciclastics rich in larger foraminifera, around the Ypresian/Lutetian boundary in the Ésera valley (South-Central Pyrenees). Although the calcareous nannofossil content in the studied interval is low, not allowing a precise Y/L boundary to be recognised, the taxa found are enough to support the chronostratigraphic attribution.

Data obtained in the Ésera valley section has improved the knowledge of larger benthic foraminifera (*Nummulites* and *Assilina*) distribution through chron C21. SBZ 11 to SBZ 12 transition took place at the lowermost C21r, as shown in previous works. SBZ 12 assemblages extend into C21n, where the SBZ 12 to SBZ 13 boundary occurs. These data, obtained in shallow marine siliciclastic facies, with *in situ* fauna, results in a shift of the SBZ 12/SBZ 13 boundary to the Lower Lutetian, younger than previously believed. Accordingly, the Ypresian/Lutetian boundary occurs in SBZ 12.

KEYWORDS | **Magnetostratigraphy. Larger benthic foraminifera. Calcareous nannofossils. Ypresian – Lutetian boundary. South-Central Pyrenean Basin.**

INTRODUCTION

The Ypresian/Lutetian (early/middle Eocene) boundary is defined by the Global Stratotype Section and Point (GSSP) of the base of the Lutetian Stage in the Gorrondatxe section (Molina *et al.*, 2011). This section is located in the Gorrondatxe Beach (Biscay synclinorium, Basque Country, Spain), within the Basque-Cantabrian Basin (Fig. 1) that has been generally referred to as the Western Pyrenees (see Barnolas and Pujalte, 2004). Previous works of the Ypresian/Lutetian Boundary Working Group (ICS) carried out on the Paleogene Pyrenean realm (South-Central Pyrenees and the Basque-Cantabrian Basin) preceded the selection of the Gorrondatxe section for its nomination (Bernaola *et al.*, 2006; Orue-Etxebarria *et al.*, 2006, 2009; Payros *et al.*, 2006, 2007, 2009a, b, 2011). The Gorrondatxe section includes a deep marine sequence of marls and pelagic limestones alternating with thin-bedded siliciclastic and calciclastic turbidites (Molina *et al.*, 2011; Payros *et al.*, 2009a).

The GSSP for the base of the Lutetian Stage was defined in a dark marly level characterized by the First Occurrence (FO) of *Blackites inflatus* (CP12a/b boundary) in the

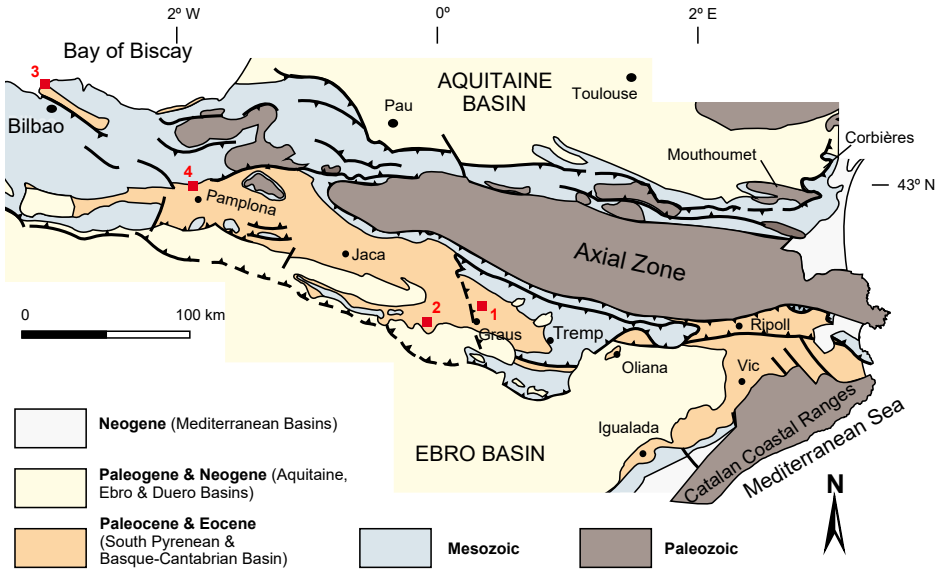

FIGURE 1. Simplified geological map of the Pyrenees including locations cited in text. 1) Besians and La Puebla de Fantova sections (this work); 2) San Pelegrín section (Rodríguez-Pintó *et al.*, 2013); 3) Gorrondatxe section (Bernaola *et al.*, 2006; Molina *et al.*, 2011; Orue-Etxebarria *et al.*, 2006, 2009; Payros *et al.*, 2007, 2009a, b); 4) Otsakar section (Payros *et al.*, 2011).

Gorrondatxe section, located in the middle of Chron 21r and represents a maximum flooding surface with a presumed global extent (Molina *et al.*, 2011). However, *B. inflatus* shows up at the base of C21n and very close to *Nannotetrina cristata* in some oceanic drills in the Pacific Ocean (Agnini *et al.*, 2006; Backman, 1986; Norris *et al.*, 2014).

In the Eocene shallow marine sequences, larger foraminifera are key forms for biostratigraphy. Their usage, since the pioneering studies in the 19th century, increased after the contributions made by Hottinger (1960) and Schaub (1981), and the definition of the Shallow Benthic Zones (SBZ) by Serra-Kiel *et al.* (1998). Nevertheless, most of the GSSPs for the Paleogene System have been defined after Serra-Kiel *et al.* (1998) work. That is the case of the Ypresian/Lutetian boundary that shifted from its previous position at the C22/C21 boundary (see Luterbacher *et al.*, 2005) to its newly defined GSSP location within C21r (Molina *et al.*, 2011). For this reason, it is necessary to review how the SBZs confront the new definition of Stage boundaries.

In the North Atlantic Ocean and western European successions, the Ypresian/Lutetian boundary is usually hampered by stratigraphic gaps (Aubry, 1995; Molina *et al.*, 2011; Payros *et al.*, 2009b). In the South Pyrenean realm, the occurrence of erosional gaps around the Y/L transition was described first by Payros *et al.* (2009b) and evidenced later in new sections (Payros *et al.*, 2011; Rodríguez-Pintó *et al.*, 2013, 2017). In the San Pelegrín section (Southern Pyrenees) (Fig. 1), which belongs to the foreland shallow carbonate platform, the Ypresian/Lutetian boundary is absent due to an erosional gap that includes at least all C21r (Rodríguez-Pintó *et al.*, 2013).

In the Gorrondatxe section, larger foraminifera appear reworked and transported from shallow water zones, which makes it difficult to assign an accurate zone attribution using the SBZ scale. Around the Y/L boundary, larger foraminifera are scarce and undoubtedly SBZ 13 forms occur within C21n (Bernaola *et al.*, 2006; Molina *et al.*, 2011; Orue-Etxebarria *et al.*, 2006), which also happens in the Otsakar section (Payros *et al.*, 2011) located as well in the Western Pyrenees (see Fig. 1). In the last two decades, the SBZ 12/SBZ 13 transition has been used as the Ypresian/Lutetian boundary in shallow water facies with larger foraminifera and absence of pelagic markers (Serra-Kiel *et al.*, 1998). In the Ésera valley in the South-Central Pyrenees, where the Cuisian (upper Ypresian) parastratotype was defined (Schaub, 1992), there is a continuous shallow-marine siliciclastic sequence rich in shallow benthic faunal assemblages of Cuisian and Luterian age (Schaub, 1981; Tosquella, 1995; Tosquella and Serra-Kiel, 1998). This section appears as an alternative locality to study the Y/L transition in shallow marine settings with abundant larger foraminiferal faunas. The results of this study, including magnetostratigraphy, larger foraminifera and calcareous nannofossils, are presented in this work.

GEOLOGICAL SETTING

The studied area is located in the Ésera valley in the south-central Pyrenees (Fig. 1). The Eocene succession in the Ésera valley belongs to the Tremp – Graus Basin. At the studied time interval, the Tremp-Graus Basin was carried piggyback (Atkinson, 1986; Atkinson and Elliot, 1985) on the South-Central Pyrenean Unit (Muñoz *et al.*, 2013; Séguret, 1972).

Shallow marine, transitional and terrestrial siliciclastic systems represent the main facies assemblages filling the Tremp–Graus Basin (Barnolas *et al.*, 2004, 2019; Chanvry *et al.*, 2018; van Eden, 1970; Nijman, 1998; Nijman and Nio, 1975, and references therein). Shallow marine carbonates are scarce in the piggyback sequence, reduced to some transgressive horizons in the Ypresian and early Lutetian successions out of the studied interval (Fig. 2).

The studied interval belongs to the Perarrúa Formation (Fm.) (Nijman and Nio, 1975), a shallow marine siliciclastic unit, rich in shallow benthic foraminifera, which includes the Ypresian-Lutetian transition (Schaub, 1981; Tosquella, 1995; Tosquella and Serra-Kiel, 1998). In the Ésera valley (Ésera road section, Fig. 3), Schaub (1992) defined the parastratotype of the Cuisian (upper Ypresian).

The Puebla de Fantova and Besians sections are located in the middle part of the Ésera valley (Eocene) succession (Fig. 3), which remained unsampled or poorly sampled for magnetostratigraphy, as exposed by Payros *et al.* (2009b) (Morillo de Liena – Santa Liestra section). They are stratigraphically younger than the Navarri section (Bentham and Burbank, 1996) (BB-1 in Fig. 3), in the lowermost Eocene units outcropping in the upper Ésera valley, below the Campanúe conglomerates. Compared to the Santa Liestra, Mesón de Pascual, and Grustán sections of Bentham and Burbank (1996) (BB-2, BB-3 and BB-4, respectively in Fig. 3), located in the lower Ésera valley, the Puebla de Fantova and Besians sections are stratigraphically older except for the Santa Liestra section that is equivalent to the uppermost part of the La Puebla de Fantova section and the lowermost part of the Besians sections.

Stratigraphy

The Perarrúa Fm. (Nijman and Nio, 1975) is a transitional and shallow marine siliciclastic unit bounded at its base and top by fluvial (red bed) units, the Castissent

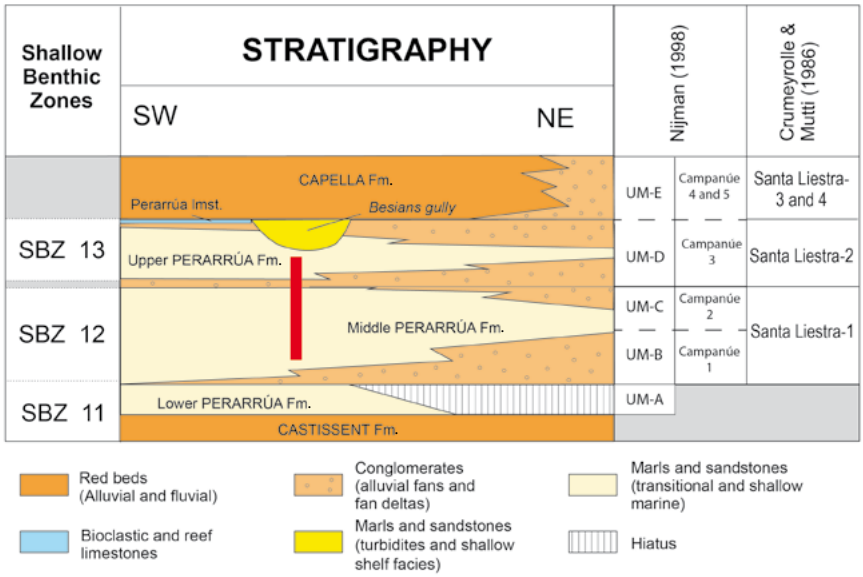

FIGURE 2. Summary stratigraphic chart of the Perarrúa and related formations (upper Ypresian–lower Lutetian) in the Tremp–Graus Basin (South-Central Pyrenees); includes in lateral boxes the informal units of Crumeyrolle and Mutti (1986) and Nijman (1998). Based on Kapellos and Schaub (1973), Nijman and Nio (1975), Schaub (1981), Crumeyrolle and Mutti (1986), Barnolas *et al.* (1991), Tosquella (1995), Nijman (1998), Robador and Zamorano (2013), López-Olmedo and Ardèvol (2016) and Teixell *et al.* (2016). The central red box indicates the stratigraphic interval corresponding to the studied sections.

and Capella formations, respectively (Fig. 2). To the north, the Perarrúa Fm. interfingers with the Campanúe and Santa Liestra conglomerates (fan-delta facies). To the southeast, the Perarrúa Fm. is lateral to a fluvial and deltaic system (Upper Montañana unit of van Eden, 1970; Nijman and Nio, 1975) developed following the Tremp-Graus basin axis (de Boer *et al.*, 1991; Crumeyrolle, 1987; Crumeyrolle and Mutti, 1986; Nijman and Nio, 1975; Nijman and Puigdefabregas, 1989) and prograding westwards. To the northwest and west, the Perarrúa Fm. evolves into a siliciclastic slope system (Mutti *et al.*, 1985, 1988) that was growing (and collapsing) on the favour of the buried lateral ramp of the South-Central Pyrenean Unit (Barnolas *et al.*, 1991; Muñoz *et al.*, 2013; Mutti *et al.*, 1988; Séguret, 1972), which delimits the Tremp-Graus (detached) to the Jaca (un-detached) basins (see Fig. 1).

As a result of the interaction of these different provenance-feeding systems, the Perarrúa Fm. shows a complex and poorly defined stratigraphy (*e.g.* Barnolas *et al.*, 1991; de Boer *et al.*, 1991; Crumeyrolle, 1987; Crumeyrolle and Mutti, 1986; Nijman and Nio, 1975). Recent geological maps (López-Olmedo and Ardèvol, 2016; Robador and Zamorano, 2013; Teixell *et al.*, 2016) help to clarify its geometrical relationships, and consequently, its stratigraphic framework (Fig. 2; 3).

In the Ésera valley section, shallow marine marls with shallow benthic foraminifera and calcareous nannofossils of a middle Cuisian age (SBZ 11; NP13/14) (Kapellos and Schaub, 1973; Payros *et al.*, 2009b) overlie the Castissent Fm. (Honegger *et al.*, 2020; Mutti *et al.*, 1988; Nijman and Nio, 1975). In this section, the Lower Campanúe conglomerate overlies these marls, which informally appears as Lower Perarrúa marls in this work (Fig. 2). The Lower Perarrúa marls die out eastwards and are absent in the Isábena valley, where the Lower Campanúe conglomerate rests unconformably (erosional unconformity) over the Castissent Fm. (Crumeyrolle, 1987; Garrido-Mejías, 1968; López-Olmedo and Ardèvol, 2016; Robador and Zamorano, 2013; Samsó, 1988). The Lower Perarrúa marls and the Lower Campanúe conglomerate belong to the Castissent-2 depositional sequence (Mutti *et al.*, 1988; Poyatos-Moré, 2014).

To the south, between the Isábena and Ésera valleys, deltaic facies of the Perarrúa Fm., with dominant paleocurrents to the west and northwest, overlie the Lower Campanúe conglomerate (López-Olmedo and Ardèvol, 2016; Teixell *et al.*, 2016). These deltaic facies laterally grade southwards to and are overlain by prodeltaic and open marine marls (Teixell *et al.*, 2016). This deepening sequence, developed over the Lower Campanúe conglomerate, appears as Middle Perarrúa unit in this work (Fig. 2).

The faunal content in this sequence indicates a late Ypresian (late Cuisian) age (SBZ 12, NP14) (Kapellos and Schaub, 1973; Schaub, 1966, 1981). The marls of the Middle Perarrúa unit are overlain abruptly by coarse sequences of flat-based sandstones and conglomerates (Santa Liestra 1-2 of Crumeyrolle and Mutti, 1986) (Fig. 2). Over this wedge of coarse-grained sediments of north-

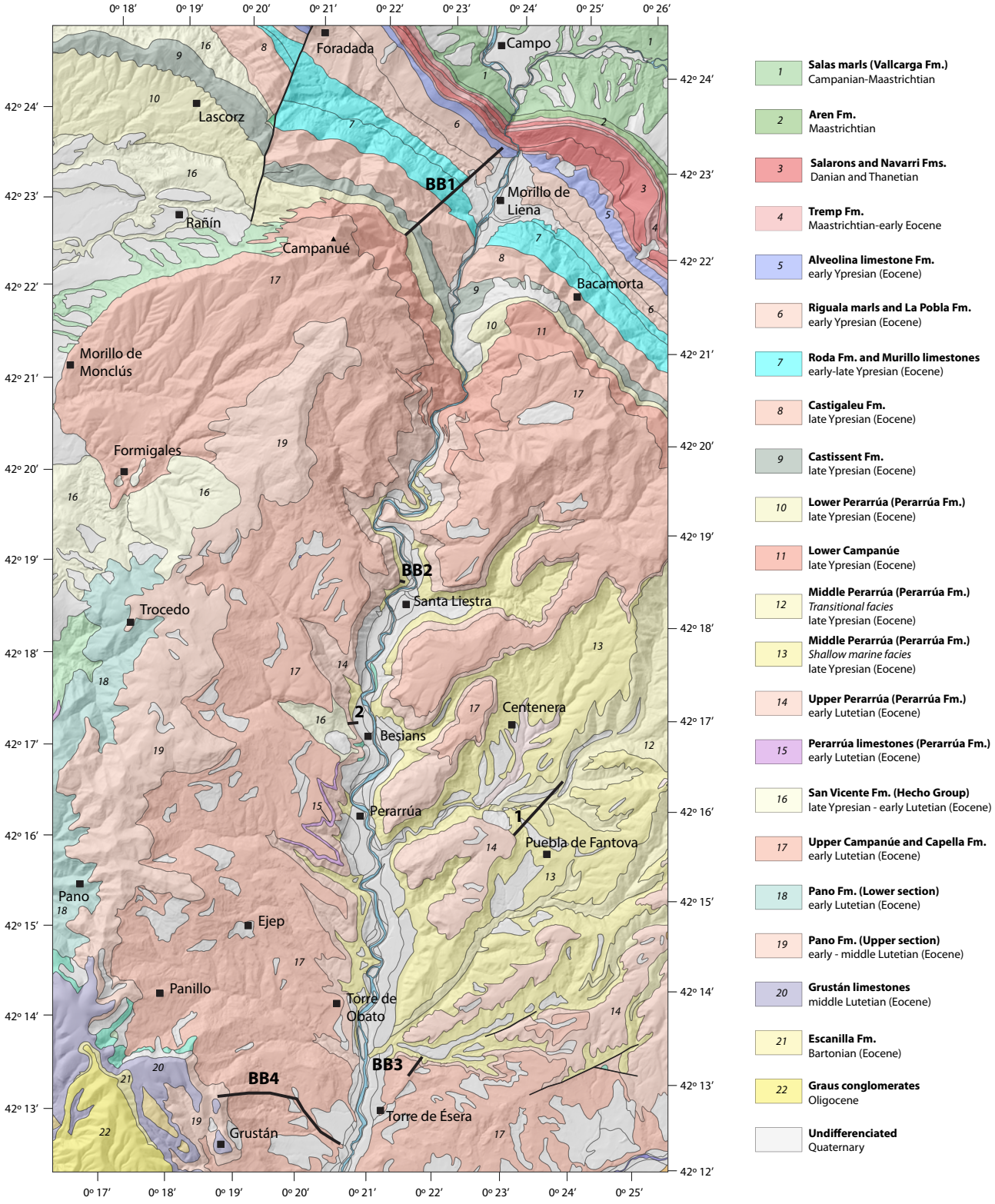

FIGURE 3. Geological map of the studied area (Ésera valley) showing the location of the 1) La Puebla de Fantova and 2) Besians sections, and the magnetostratigraphic sections studied previously by Bentham and Burbank (1996) and referred in text (BB1= Navarri section; BB2= Santa Liestra section; BB3= Mesón de Pascual section; BB4= Grustán section). Geological map modified from Teixell *et al.* (2016) and Robador and Zamorano (2013).

provenance, the sequence becomes progressively finer-grained and includes abundant neritic faunas, in a deepening upward (transgressive) trend (Crumeyrolle, 1987). This deepening upward sequence, referred to as Upper Perarrúa in this work, leads up to a slope truncation filled by deep-water mudstones, muddy slumps and turbidite sandstones (Besians gully) (Barnolas *et al.*, 1991; Crumeyrolle, 1987; Crumeyrolle and Mutti, 1986; Rumpff and de Boer, 1985). According to Tosquella (1995), the age of the Upper Perarrúa unit is early Lutetian, including *Nummulites gallensis*, *N. lehneri*, *N.* aff. *obesus*, *N.* aff. *verneuli*, *N. praelorioli*, *N. laevigatus* and *N.* aff. *Messinae* in its lower part and *Nummulites* aff. *obesus*, *N. lehneri*, *N.* aff. *boussaci*, *N. laevigatus*, *N. messinae*, *N. britannicus*, *Assilina* aff. *maior*, *A. spira abrardi* and *A.* aff. *Exponens* in their upper part of the N. laevigatus and A. spira abrardi biozones of Schaub (1981). The sedimentary filling of the Besians gully also hosts SBZ 13 (lower Lutetian) fauna (Tosquella, 1995; Tosquella, in Barnolas *et al.*, 1991).

The upper boundary of the Perarrúa Fm. consists of an abrupt transition to the fluvial red bed facies of the Capella Fm. (Cuevas-Gozalo, 1989; Nijman and Nio, 1975) (Fig. 2). To the north (Ésera valley outcrops), this transition follows a sharp irruption of coarse alluvial fan conglomerates (upper prograding wedge of Santa Liestra-2 of Crumeyrolle, 1987) (Fig. 2), which results in a complex sequence of conglomerates, sand bars and bioclastic sands that include coralgal limestones, interpreted as barrier-bar complexes (Nijman and Nio, 1975).

MATERIALS AND METHODS

The Puebla de Fantova and Besians sections were logged and sampled for this study. The Puebla de Fantova section is located along the local road to Centenera village (Fig. 3). The base of this section corresponds to the delta front facies of the Middle Perarrúa unit at the Casa del Molino bridge (cartographic unit 22 of Teixell *et al.*, 2016; 12 in Fig. 3) and continues close to the road between the shallow marine marls and sandstones of this unit (cartographic unit 23 of Teixell *et al.*, 2016; 13 in Fig. 3). The Puebla de Fantova section ends within the lowest sandstone levels of the Upper Perarrúa unit in the Ermita hill, close to La Puebla de Fantova village (base of cartographic unit 24 of Teixell *et al.*, 2016; 14 in Fig. 3). The contact between the Middle and Upper Perarrúa units is sharp, marked by the base of a regional cartographic reference level (Teixell *et al.*, 2016), which works as the correlation level between the Puebla de Fantova and Besians sections. This contact is interpreted as the result of an abrupt input of fan delta deposits. The base of the second section (Besians section), near the Besians village (Fig. 3), is located in the upper part of the Middle Perarrúa marls (cartographic unit 23 of Teixell *et al.*, 2016; 13 in Fig. 3) and includes the lower part of the Upper Perarrúa unit (cartographic unit 24 of Teixell *et al.*, 2016; 14 in Fig. 3) where several levels with lower Lutetian shallow benthic larger foraminifera where recognised (Tosquella, 1995). The lower part of the Besians section (first 75m) is made up of fan-delta sandstones and conglomerates of northern provenance (Santa Liestra 1-2 transition of Crumeyrolle and Mutti, 1986, which are interpreted as the product of reworking of northern derived coarse-grained sediment, resulting in a succession of barrier-bar complexes (Nijman and Nio, 1975). The upper part of this stratigraphic profile corresponds to more open marine facies, rich in larger foraminifera, including marls, siltstones and fine-grained sandstones. The upper boundary of this sequence is the Besians gully truncation, which marks also the top of the studied succession.

Biostratigraphy: Sampling and procedures

A total of sixteen samples were collected to study the larger foraminiferal assemblages (*Nummulites*, *Assilina* and *Alveolina*) in the studied stratigraphic interval, nine along the Puebla de Fantova section (Fig. 4) and seven along the Besians section (Fig. 5). In all the samples the specimens were isolated and prepared accordingly to study its surface features and equatorial and axial sections.

The samples were disaggregated in an oxygen peroxide and Na_2CO_3 solution, and the fine sediment removed using 1.0-, 0.5- and 0.2-mm mesh sieves. The larger foraminifera were picked from the washed residues, each specimen split by its equatorial section, and studied and measured under a light microscope at 40x magnification. The systematic approach in this work follows the taxonomic criteria used by Schaub (1951, 1966, 1981), Tosquella (1995), Tosquella and Serra-Kiel (1998) and Hottinger (1960, 1974). The studied material is housed at the Museu de Ciències Naturals de Barcelona with the following register number: F 1m= MGB 90339; F 2m= MGB 90340; F 3m= MGB 90341; F 4m= MGB 90342; F 5m= MGB 90343, F 6m= MGB 90344; F 7m= MGB 90345; F 8m= MGB 90346; Be 1= MGB 90347; Be 2= MGB 90348; Be 3= MGB 90349; Be 4= MGB 90350; Be 5= MGB 90351; Be 6= MGB 90352; Be 7= MGB 90353.

Calcareous nannofossil assemblages were analysed in 18 samples; thirteen were collected in the Puebla de Fantova section and five in the Besians section (Fig. 4; 5, for sample location). All the samples were prepared from unprocessed material as smear slide using standard procedure (Bown and Young, 1998). The nannofossil biostratigraphy presented here is based on the examination of the samples with a Zeiss Axioplan petrographic microscope at varying magnification (x 1000-x 1600), using plain and cross-polarized light. Due to the scarcity of

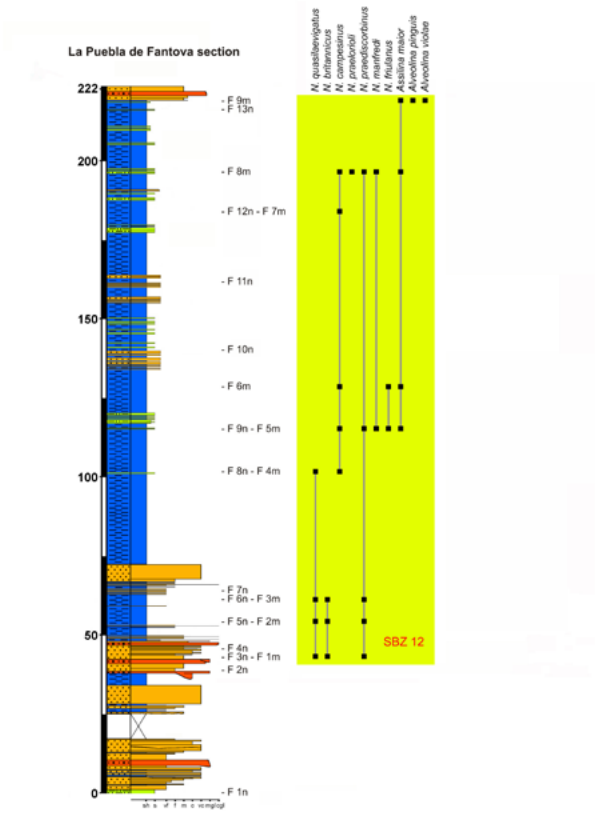

FIGURE 4. La Puebla de Fantova section. Location of biostratigraphic samples (m for larger foraminifera and n for calcareous nannofossils) and distribution of larger foraminiferal species. Legend in Figure 5.

calcareous nannofossils in the studied samples, more than 5 traverses were analysed to detect rare species with key biostratigraphic value. The standard schemes of Martini (1971) and Okada and Bukry (1980) and the standard taxonomy for Cenozoic calcareous nannofossils (Agnini *et al.*, 2014; Bown, 2005; Perch-Nielsen, 1985; Young and Bown, 1997) have been adopted for this study. Table 1 summarizes the obtained results.

Magnetostratigraphy: Sampling and procedures

A total of 99 paleomagnetic samples were drilled at the two sections: a standard core was taken at 4-6m stratigraphic intervals at Puebla de Fantova (50 cores along the 220m-thick stratigraphic section), and 2-3m at Besians (49 cores along 125m-thick stratigraphic section). For these tasks, a water-cooled gasoline-powered drilling machine was used to avoid disturbance on the paleomagnetic record. Cores were in-situ oriented using a clinometer attached to a magnetic compass.

Once in the laboratory, cores were cut in standard specimens of 10.4cm^3 and relabelled for further analyses. Magnetic measurements were taken in the Laboratory of Paleomagnetism of the Montanuniversität Leoben (Austria). An SRM-755 cryogenic magnetometer (2G) and an MMTD60 (by Magnetic Measurements Ltd) thermal demagnetizer were used to carry out the stepwise thermal (TH) demagnetization of samples. A 2G Pulse magnetizer was used to impart the samples with an Isothermal Remanent Magnetization (3 axes-IRM). Finally, an MFK1 Multifunction Bridge (by AGICO) was used for bulk susceptibility monitoring during the thermal treatment.

The magnetic Local Polarity Sequence (LPS) in the studied profiles was built from more than 100 stepwise thermal demagnetizations. In every specimen, up to 11 steps were studied in the thermal demagnetization

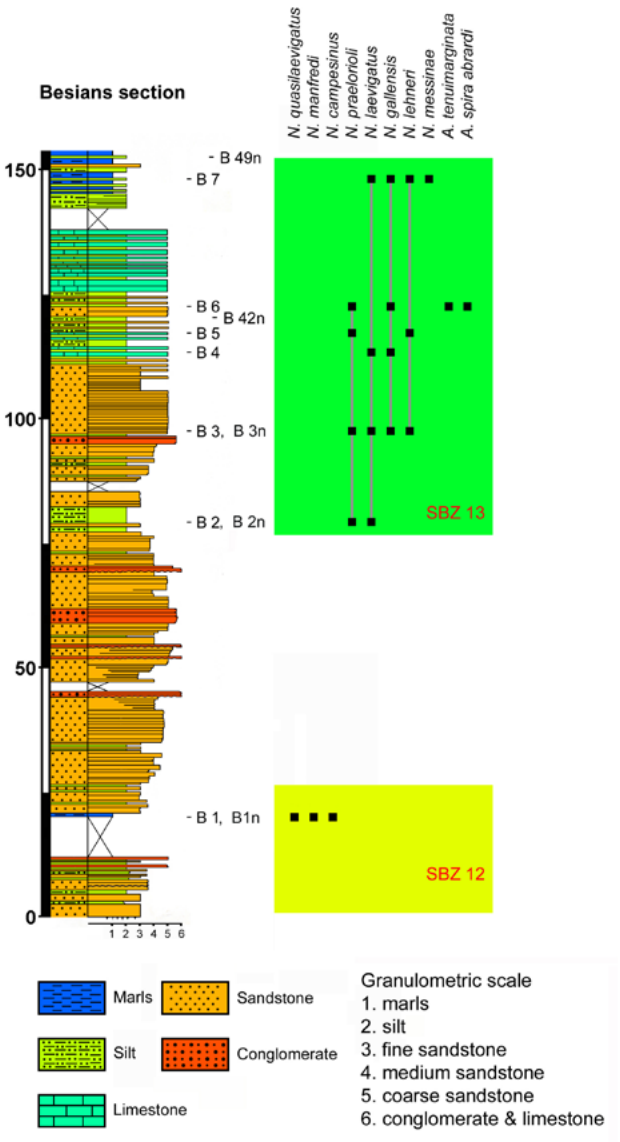

FIGURE 5. Besians section. Location of biostratigraphic samples (B+ number for larger foraminifera; B+ number + n for calcareous nannofossils) and distribution of larger foraminiferal species.

TABLE 1. Upper part: Range chart of selected calcareous nannofossils identified in La Puebla de Fantova and Besians sections. Total abundance of calcareous nannofossils expressed in specimens per field of view. PP: very poor preservation, P: poor preservation, M: moderate preservation. In red calcareous nannofossil species recorded by Kapellos and Schaub (1973) in samples 24 and 102 in the Campo section. Lower part: Photographs of selected calcareous nannofossil taxa from La Puebla de Fantova section. The scale bar represents 5µm in photographs 1-5. 1) 5-rayed *Discoaster sublodoensis*, sample F 10n. 2) 6-rayed *Discoaster sublodoensis*, sample F 10n. 3) *Ericsonia formosa*, sample F 7n. 4) *Reticulofenestra dictyoda*, sample F 11n, 5) *Discoaster barbadiensis*, sample, F 1n. 6-7) General view of samples F 10n and F 7n showing the high abundance of reworked Cretaceous species

	Sample	Abundance (specimens per field of view)	Preservation	Reworked Cretaceous specimens	*Braarudosphaera bigelowii*	*Campylosphaera dela*	*Chiasmolithus solitus*	*Chiasmolithus consuetus*	*Chiasmolithus grandis*	*Ch.* sp. aff. *quadratus* = *Nannotetrina cristata*	*Chiphragmalithus calathus*	*Clausicoccus* spp.	*Coccolithus crassus*	*Coccolithus pelagicus*	*Cyclicargolithus florindanus*	*Cyclicargolithus luminis*	*Discoaster barbadiensis*	*Discoaster deflandrei*	*Discoaster distinctus*	*Discoaster kuepperi*	*Discoaster lodoensis*	*Discoaster saipanensis*	*Discoaster sublodoensis*	*Discoaster* spp.	*Discolithina* sp.	*Ericsonia formosa*	*Girgisia gammation*	*M. tribrachiatus* = *Tribrachiatus orthostylus*	*Neococcolithes dubius*	*Prinsiaceae* < ca. 4µm	*Pseudotriquetrorhabdulus inversus*	*Reticulofenestra* spp.	*Dictyococcites* spp.	*Sphenolithus* spp.	*Toweius* spp.	*Transversopontis pulcher*	*Zygrhablithus bijugatus*	Calcareous nannofossil Zones: Martini (1971)	Okada and Bukry (1980)
Besian Section	B49n	<1	PP	x											Only reworked Cretaceous species																						uncertain	
	B42n	<1	PP	x																																		
	B3n	<1	PP	x																												x					NP14	CP12b
	B2n	<1	PP	x											cf.																	x						
	K102	-	-	-		x		x	x	x							x	x			x	x	x		x										x		
	B1n	<1	PP	x										x																		x				uncertain	
La Puebla de Fantova Section	F13n	8	M	x									x	x	x	x								x						cf.	x	x				x	NP14	CP12a
	K24	-	-	-	x			x	x		x						x		x			x					x	x								x		
	F12n	1	P	x									x		x																x							
	F11n	3	P-M	x			x					cf.	x	x										x			cf.					x	x					
	F10n	3	M	x	x		x					x	x			x					cf.		x	x									x	x				
	F9n	1	P	x							x		x		x	x																	x					
	F8n	2	P	x									x		x																		x					
	F7 n	21	M	x				x				x	x	x	cf.	x	x			x		x				x				x		x	x				x	
	F6n	<1	PP	x										x																			x					x	
	F5n	<1	PP	x										x										x									x					
	F4n	<1	PP	x										x																			x		cf.			
	F3n	<1	PP	x																													x	x				
	F2n	<1	PP	x										x																			x					
	F1n	2	M	x	x	x						x		x		x	x							x						x		x			x		x	

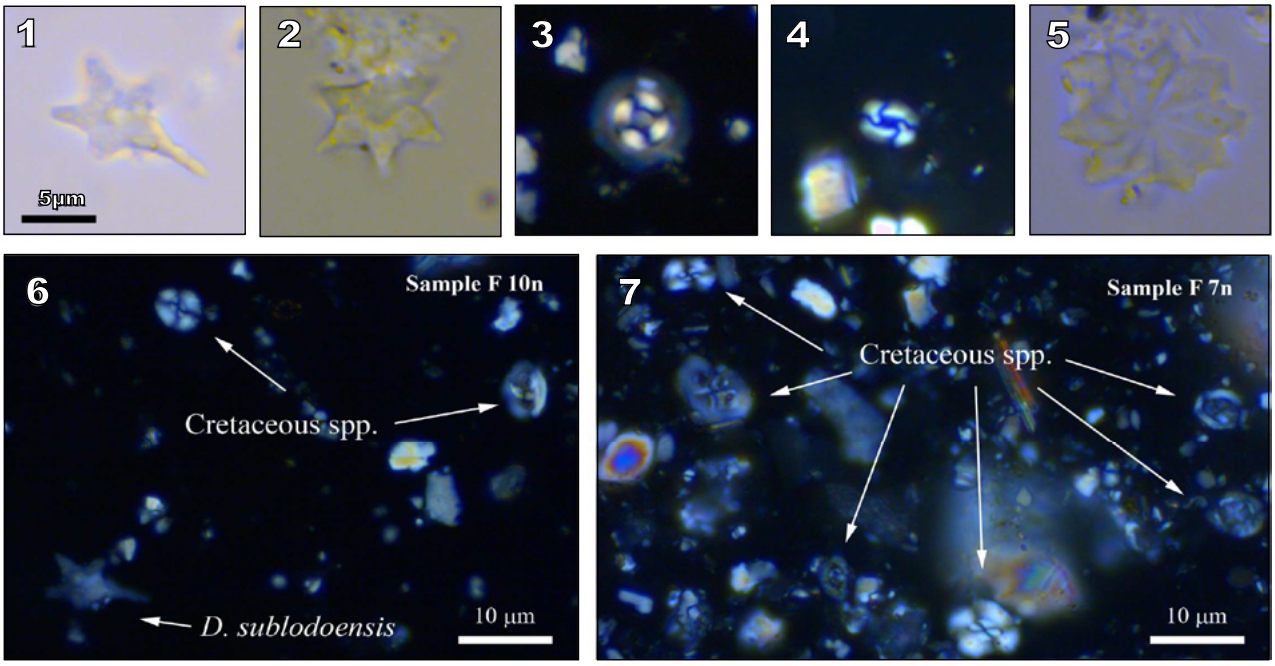

routines reaching temperatures up to 500°C. Steps starting at 20°C, 180°C, 240°C, then every 30°-40° up to 500°C. Paleomagnetic directions were fitted by means of end-point and Principal Component Analyses (PCA; Kirschvink, 1980) using the VPD software (Ramón *et al.*, 2017).

Paleomagnetic directions were grouped into three different types according to their quality and reliability. Type 1 vectors display a good definition (usually estimation errors below 15°) and address undoubtedly to the origin. Type 2 vectors may be poorer (errors ≥15°), but display an unambiguous polarity. Type 3 vectors are weaker and/or noisier directions. The LPS profile was only characterized by type 1 and 2 samples to ensure the reliability of the magnetostratigraphic record. Profile directional means were calculated using Fisher's (1953) and Bingham's (1974) statistics under the software Stereonet version 9.9.1 (Allmendinger *et al.*, 2013; Cardozo and Allmendinger, 2013).

Three axis-IRM acquisition and its TH demagnetization (Lowrie's 1990 test) were applied for a set of samples aiming to obtain information about the coercivity of the magnetic minerals present in the rocks. For this, a peak field was applied in each of the three main axes. Applied fields were: Z: 2.0; Y: 0.4 and X: 0.012 Tesla, consecutively. Then, the thermal demagnetization routine was performed in thirteen steps from 20°C up to 680°C.

RESULTS

Biostratigraphic data

Larger foraminifera

Biostratigraphic material from La Puebla de Fantova and Besians sections (Figs. 4; 5 respectively) is described in detail in this section (Figs. 6; 7; 8; 9). In the Puebla de Fantova section (Fig. 4), samples F 1m, F 2m and F 3m contain *Nummulites quasilaevigatus* PAVLOVEC, 1974, *N. britannicus* HANTKEN, 1873 sensu Hottinger and Schaub, 1964 and *N. praediscorbinus* SCHAUB, 1981. This stratigraphic interval comprises the paleomagnetic samples 8 to 24, and the calcareous nannofossils samples F 3n to F 6n. Sample F 4m (equivalent to 36-37 and F 8n) contains *N. quasilaevigatus* and *N. campesinus* SCHAUB, 1966. Sample F 5m (equivalent to F 9n) contains *Assilina maior* DE LA HARPE, 1883, *N. praelorioli* HERB AND SCHAUB, 1963, *N. praediscorbinus*, *N. manfredi* SCHAUB, 1966, *N. campesinus* and *N. friulanus* SCHAUB, 1962. Sample F 6m contains *Assilina maior*, *N. friulanus* and *N. campesinus*. Sample F 7m (equivalent to F 12n) contains *N. campesinus*. Sample F 8m contains *Assilina maior*, *N. praelorioli*, *N. praediscorbinus*, *N. manfredi* and *N. campesinus*, and sample F 9m (equivalent to F 13n and 50) contains *Alveolina violae* CHECCHIA-RISPOLI, 1905, *Alveolina pinguis* HOTTINGER, 1960 and *Assilina maior*.

In the Besians section (Figure 5) sample B 1 (equivalent to B 1n) contains *N. quasilaevigatus*, *N. manfredi* and *N. campesinus*. Sample B 2 (equivalent to B 2n and 28-30) contains *N. praelorioli*, *N. laevigatus* (BRUGUIÈRE, 1792) and *N. gallensis* HEIM, 1908. Sample B 3 contains *N. gallensis*, *N. lehneri* SCHAUB, 1962, *N. praelorioli* and *N. laevigatus*. Sample B 4 contains *N. laevigatus* and *N. gallensis*. Sample B 5 contains *N. praelorioli* and *N. lehneri*. Sample B 6 contains *N. praelorioli*, *N. gallensis*, *Assilina tenuimarginata* and *Assilina spira abrardi* SCHAUB, 1981, and sample B 7 contains *N. praelorioli*, *N. laevigatus*, *N. messinae* SCHAUB, 1981, *N. gallensis* and *N. lehneri*.

Calcareous nannofossils

The studied samples were of poor quality for the calcareous nannofossil study due to the poor preservation and low abundance of the autochthonous specimens and the presence of abundant reworked Cretaceous specimens, which represent the 60-95% of the total assemblage in all the samples (Table 1).

The lower samples of La Puebla de Fantova section (F 1n-F 6n) (Fig. 4) are almost barren of calcareous nannofossils. Only the sample F 1n shows more than 1 specimen per field of view (spp./f.v.). The observed specimens are usually broken and show traces of dissolution. In this interval, the reworked, dissolution resistant, Cretaceous species of the genera *Eiffellithus*, *Watznaueria* and *Prediscosphaera* dominate the assemblages. The more prevalent autochthonous species are *Coccolithus pelagicus* and representatives of the genera *Cyclicargolithus* and *Reticulofenestra* including the species *Reticulofenestra dictyoda*. The calcareous nannofossil abundance and preservation improves up-section. Sample F 7n shows 21 spp/f.v. but almost all the identified specimens are reworked Cretaceous species (Table 1). From sample F 8n up to the top of the section (sample F 13n), the calcareous nannofossil abundance ranges from 1 to 8 spp./f.v. In this samples the reworked Cretaceous specimens are more abundant than the autochthonous specimens and the preservation varies from moderate to poor. The autochthonous calcareous nannofossil assemblage is still dominated by *Coccolithus pelagicus* and species of *Reticulofenestra* and *Cyclicargolithus*. The presence of 5-rayed *Discoaster sublodoensis* in sample F 10n (Table 1) is noteworthy.

The five samples of the Besians section (Fig. 5) are very poor. In samples B 1n to B 3n only 1 spp/f.v. was recorded. Reworked Cretaceous specimens dominate the

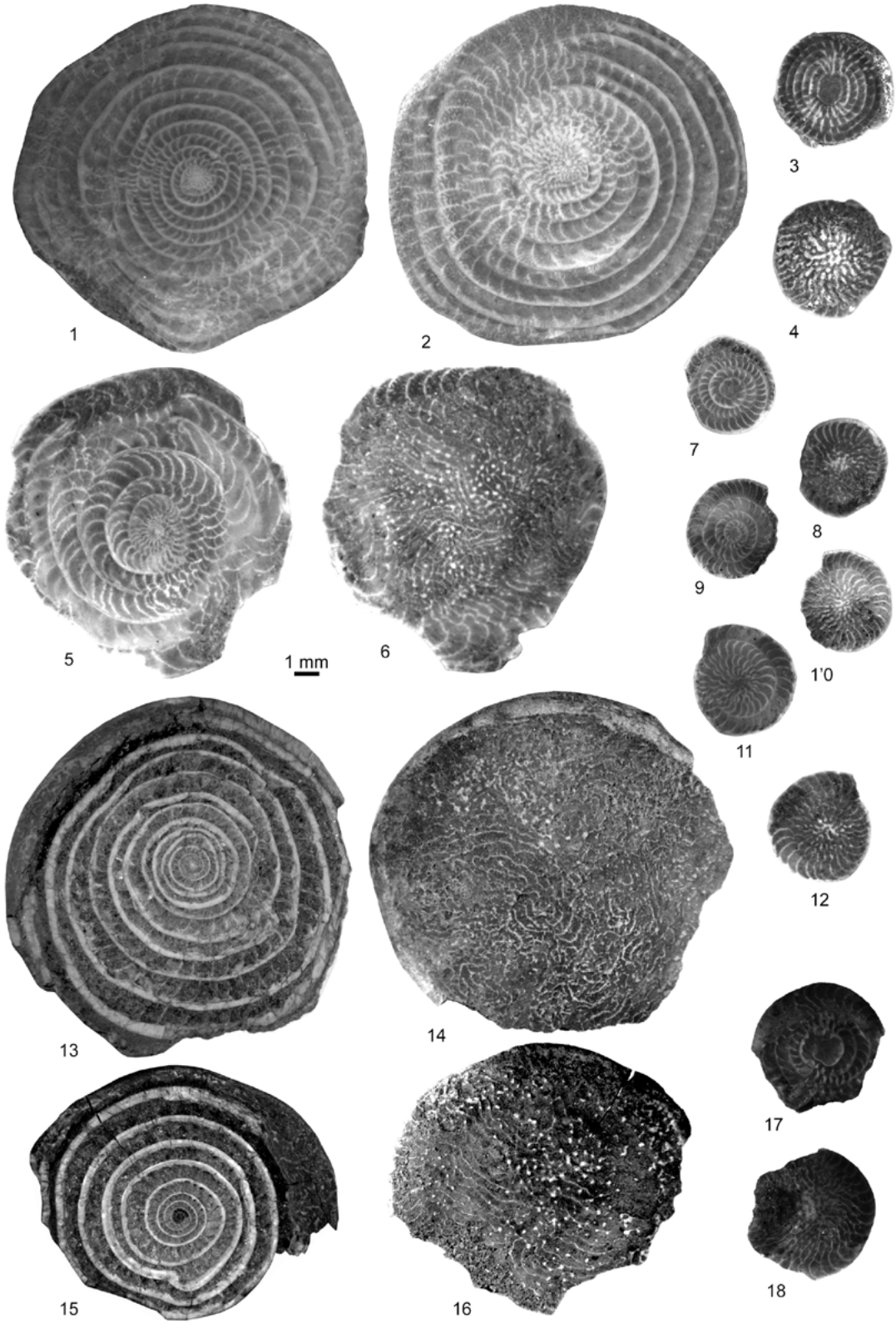

FIGURE 6. *Nummulites quasilaevigatus* PAVLOVEC, 1974: 1-2) B-forms, equatorial sections; 3-4) A-forms equatorial section and external view. Specimen 1 from sample F 1m; specimens 2-4 from sample F 4m. *Nummulites britannicus* HANTKEN, 1873 in Hottinger and Schaub, 1964: 5-6) B-forms, equatorial section and external view; 7-12) A-forms, equatorial sections and external views. Specimens from sample F 3m. *Nummulites manfredi* SCHAUB, 1966: 13-16) B-forms, equatorial sections and external views; 17-18) A-forms, equatorial section and external view. Specimens from F 5m.

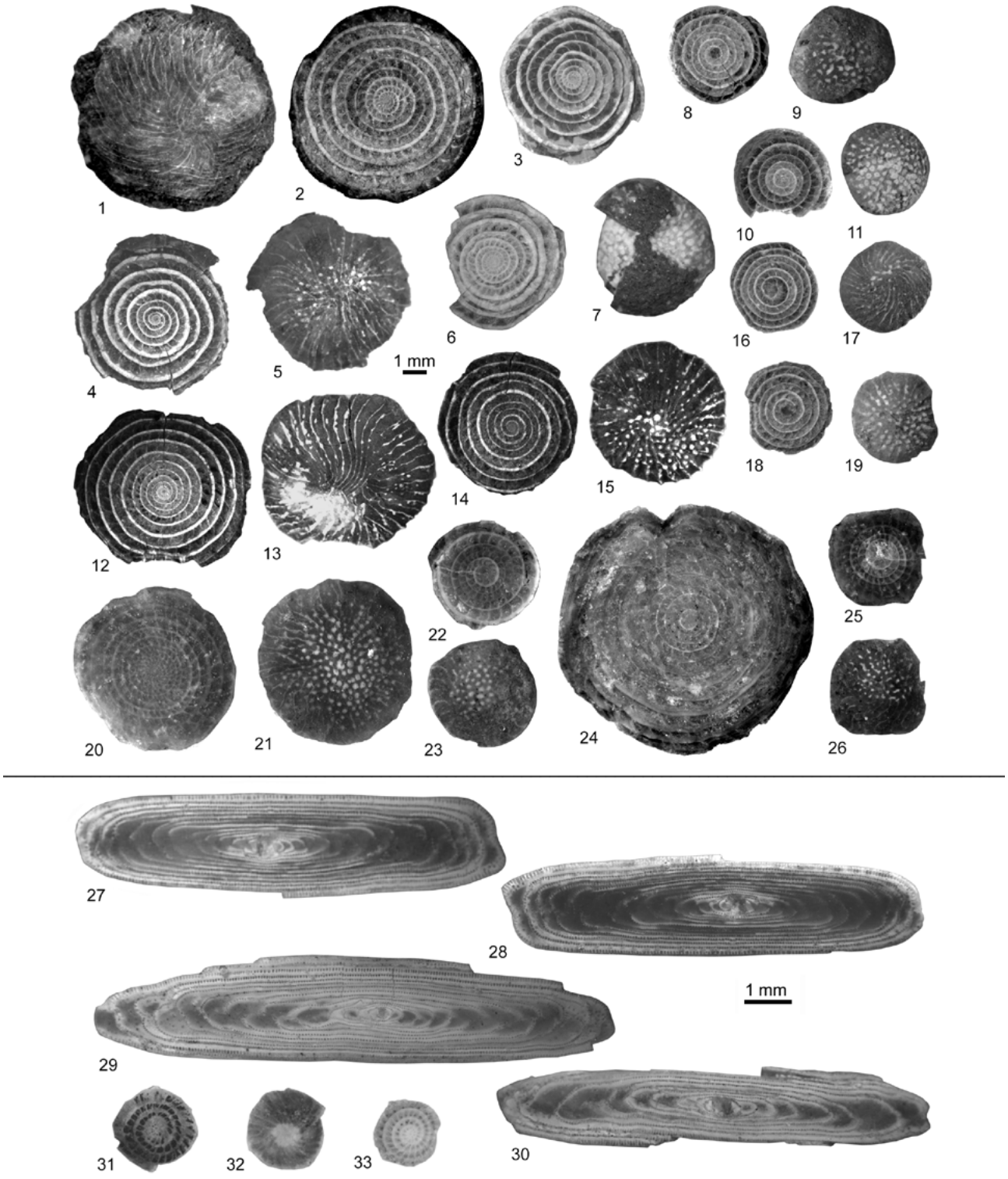

FIGURE 7. *Nummulites campesinus* SCHAUB, 1966: 1-7) B-forms, equatorial sections and external views; 8-11) A-forms, equatorial sections and external views. Specimens 1-2, 4-5 from sample F 5m; specimens 3, 6-11 from sample F 7m. *Nummulites friulanus* SCHAUB, 1962: 12-15) B-forms, equatorial sections and external views; 16-19) A-forms, equatorial sections and external views. Specimens from sample F 6m. *Nummulites gallensis* HEIM, 1908: 20-21) B-forms, equatorial section and external view; 22-23) A-forms, equatorial section and external view. Specimens from sample B 6. *Nummulites lehneri* SCHAUB, 1962: 24) B-form, equatorial section; 25-26) A-forms, equatorial section and external view. Specimens from sample B 7. *Alveolina violae* CHECCHIA-RISPOLI, 1905: 27-28) A-forms, axial sections. Specimens from sample F 9m. *Alveolina pinguis* HOTTINGER, 1960. 29-30) A-forms, axial sections. Specimens from sample F 9m. *Nummulites praediscorbinus* SCHAUB, 1981: 31-33) A-forms, equatorial sections and external view. Specimens from sample F 2m.

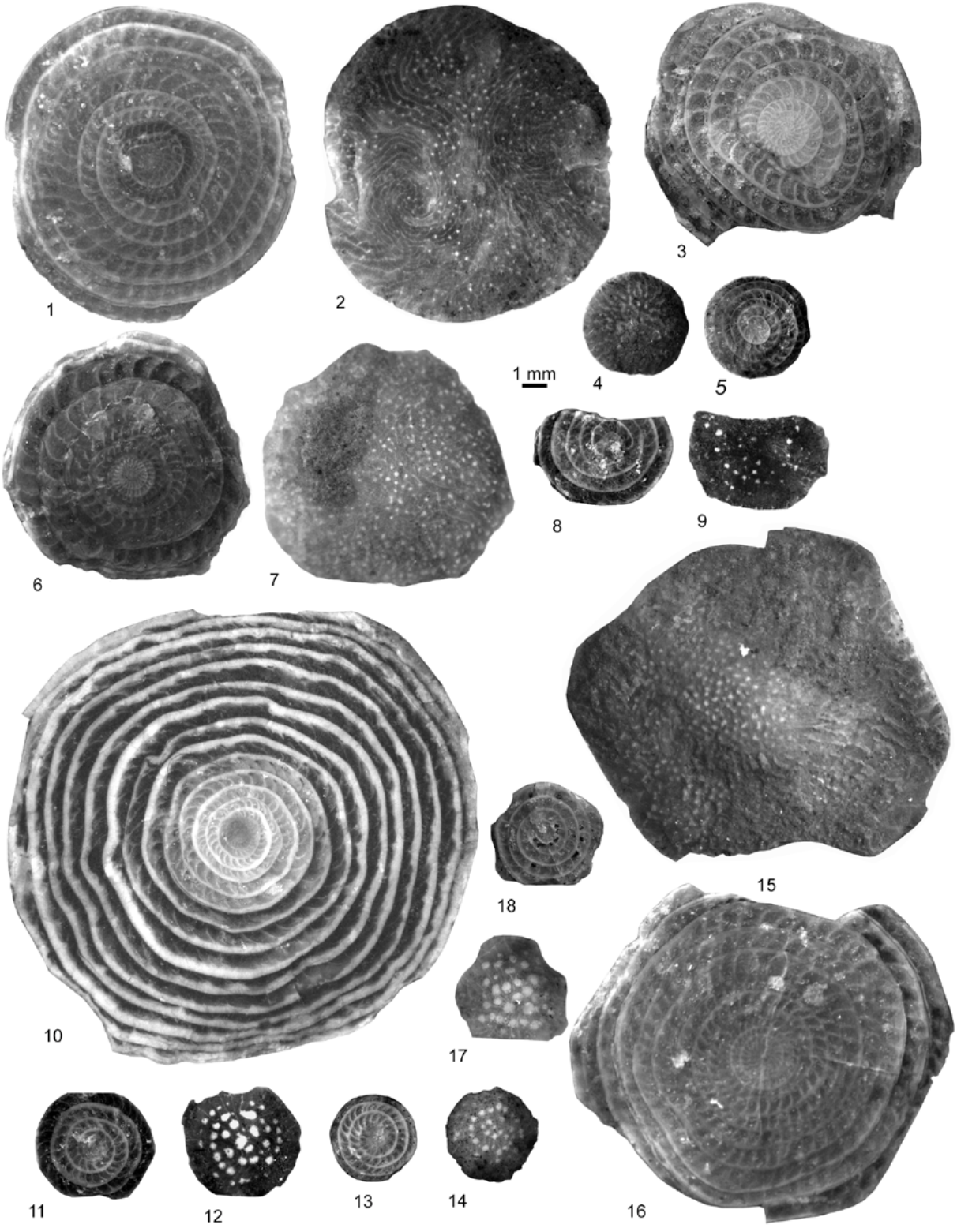

FIGURE 8. *Nummulites laevigatus* (BRUGUIÈRE, 1792): 1-3, 15-16) B-forms, equatorial sections and external view;. 4-5) A-forms, equatorial section and external view. Specimens from sample B 7; specimens 4-5 from sample B 2. *Nummulites messinae* SCHAUB, 1981: 6-7) B-forms, equatorial section and external view; 8-9) A-forms, equatorial section and external view. Specimens from sample B 7. *Nummulites praelorioli* HERB AND SCHAUB, 1963: 10) B-form, equatorial section; 11-14) A-forms, equatorial sections and external views. Specimens 10-12 from sample B 7; specimens 13-14 from sample B 6.

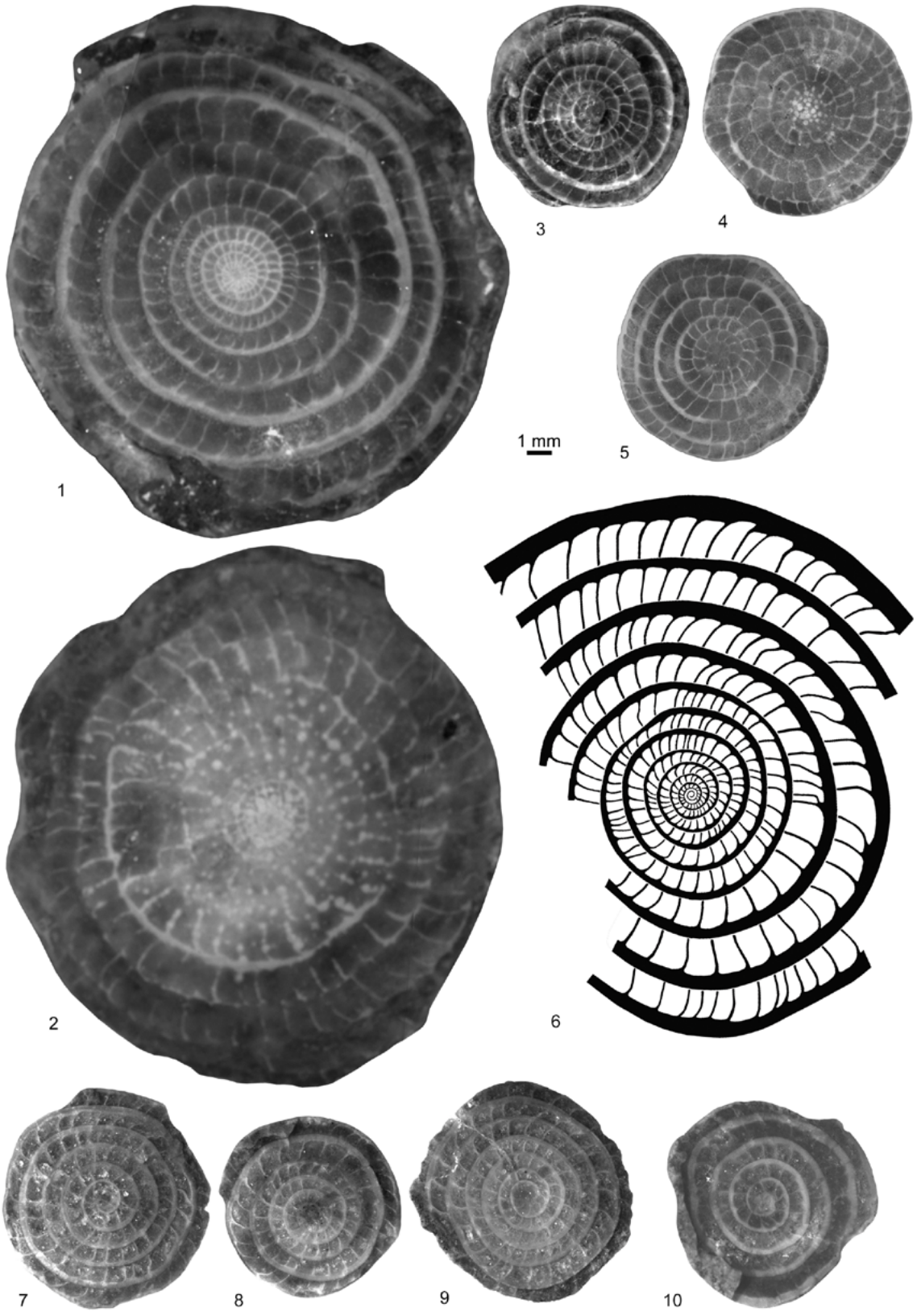

FIGURE 9. *Assilina maior* DE LA HARPE, 1883: 1-2) B-forms, equatorial section and external view; 3-5) A-forms equatorial sections and external view. Specimens 1 and 2 from sample F 9m; specimens 3-5 from sample F 6m. *Assilina spira abrardi* SCHAUB, 1981: 6) B-form, equatorial section, specimen from sample B 6, drawing on photography. *Assilina tenuimarginata* HEIM, 1908: 7-10) A-forms, equatorial sections. Specimens from sample B 6.

assemblages and only a few representatives of the genera *Reticulofenestra*, *Coccolithus* and *Discoaster* (fragments) were found. Samples B 42n and B 49n were almost barren of calcareous nannofossils and the few specimens found were reworked Cretaceous specimens.

Paleomagnetic and rock magnetism data

Lowrie's (1990) tests performed on several samples from both profiles (Fig. 10) reveal the presence of soft, medium and high coercivity range, although soft and medium coercivity curves dominate quantitatively at diagrams. The soft coercivity curves decay completely about 580°C clearly indicating the presence of magnetite as the main magnetic carrier. Medium coercivity curves often fall around 300-350°C and suggest the occurrence of undifferentiated sulphides (likely greigite). Moreover the BE02 sample shows a final decay at a higher temperature (about 675°C), showing a medium-hard coercivity mineral behaviour (likely hematite). Finally, the high coercivity curve, generally decays about 675°C, but also shows decay at very low temperatures in very few cases (decay before 200°C, in some cases, such as in FA22) due to the presence of some goethite. All these data together with demagnetization features, seems to indicate the presence of magnetite and undifferentiated sulphides as the main carriers, accompanied by the presence of hard coercivity minerals in some few cases. These results are in agreement with early diagenetic re-equilibrium of magnetite and greigite that may result, despite some noise, in reliable primary records of the magnetic field (Larrasoaña *et al.*, 2003) as it has been demonstrated in many magnetostratigraphic studies of the South Pyrenean basin (Garcés *et al.*, 2020 and references therein).

Stepwise thermal demagnetizations as displayed in Zijderveld's (1967) diagrams (Fig. 10) allowed fitting reliable directions from 82 samples. Data from remaining samples were ruled out because of weak Natural Remanent Magnetization (NRM) intensity or erratic demagnetization (type 3). Characteristic Remanent Magnetization (ChRM) directions were fitted with 6-7 steps on average. Most of samples were fully demagnetized up to 500°C, and in some samples authigenic magnetic minerals (magnetite) grew up during their heating in the oven beyond 400°C, as revealed by significant increments of susceptibility (as in many similar Pyrenean rocks; Pueyo *et al.*, 2002; Larrasoaña *et al.*, 2003). Some samples showed very weak magnetizations, and higher demagnetization steps were not considered in further calculations.

As a general rule, Zijderveld diagrams (Fig. 10) show two magnetic components: a viscous low temperature component up to 180-240°C, in average, very similar to the present geomagnetic field (DEC: 358, INC: 53); and a high temperature component from ~200°C up to 420 -570°C (when possible). This component displayed normal and reversed directions with linear trajectories very often decaying to the origin (type 1) and it has been considered the ChRM used to build the LPS's.

The entire demagnetization dataset (Fig. 11) shows NRM ranging between 0.114 and 1.619mA/m (mean of 0.51mA/m and a standard deviation of 0.31mA/m). Besides, susceptibilities fell within the paramagnetic domain defined in Pyrenean rocks (Pocoví *et al.*, 2014; Pueyo-Anchuela *et al.*, 2013) and ranged from 2 to $94*10^{-6}$ S.I. (averaged out $37*10^{-6}$ S.I., and standard deviation of $18.96*10^{-6}$ S.I.).

From a directional point of view (only type 1 and 2 samples), the ChRMs in the lower hemisphere and merging both profiles together, are well-grouped After Bedding Correction (ABC) and display a robust Fisher distribution and expected inclinations; Dec: 020, Inc: 61 (α95: 8°, k; 4.8 and R: 0.7945) in agreement to data of the South Pyrenean Central Unit (Beamud *et al.*, 2004; Dinarés-Turell, 1992) and to the closer Ainsa oblique zone (Muñoz *et al.*, 2013; Oliva-Urcia and Pueyo, 2019 and references therein).

Once the data are restored to the paleohorizontal, the normal polarity dominates the dataset. Mean Fisher statistics (Table 2) by polarity are Dec: 012, Inc: 64 (α95: 9.3°, k: 4.8) for the normal polarity directions (61points) and 215, -52 (α95: 15.6° and k: 5.1) for the reverse ones (21 points). The fold and reversal tests yield non-significant results if our own dataset is used alone; partially (fold test) because of the lack of enough bedding dip differences and also (reversal test) because of the small number of reverse vectors. In any case, the pseudo-antiparallel character of both polarities (Fig. 11), together with several previous works with well-proven primary attributes in the southern Pyrenees (see recent overviews by Garcés *et al.*, 2020; Oliva-Urcia and Pueyo, 2019), allow us to be confident about the primary character of the dataset.

Studied sections were based on a detailed stratigraphic study, measured sections with enough sampling density to characterize the LPS, complete TH demagnetization and ChRMs fitted with standard methods and fully published (dec, inc, Virtual Geomagnetic Poles (VGP) latitude) apart from the polarity log, rock magnetism analyses to determine the magnetic carriers, pseudo-antipodal means (after restoration) with expected inclinations and, despite the lack of our own fold test, plenty data in the region supporting the primary character of the magnetization. Therefore, and following the van der Voo (1990) and Opdyke and Channel (1996) criteria, the results obtained in La Puebla de Fantova and Besians are reliable to propose a chronostratigraphic age model together with the biostratigraphic data introduced in this paper.

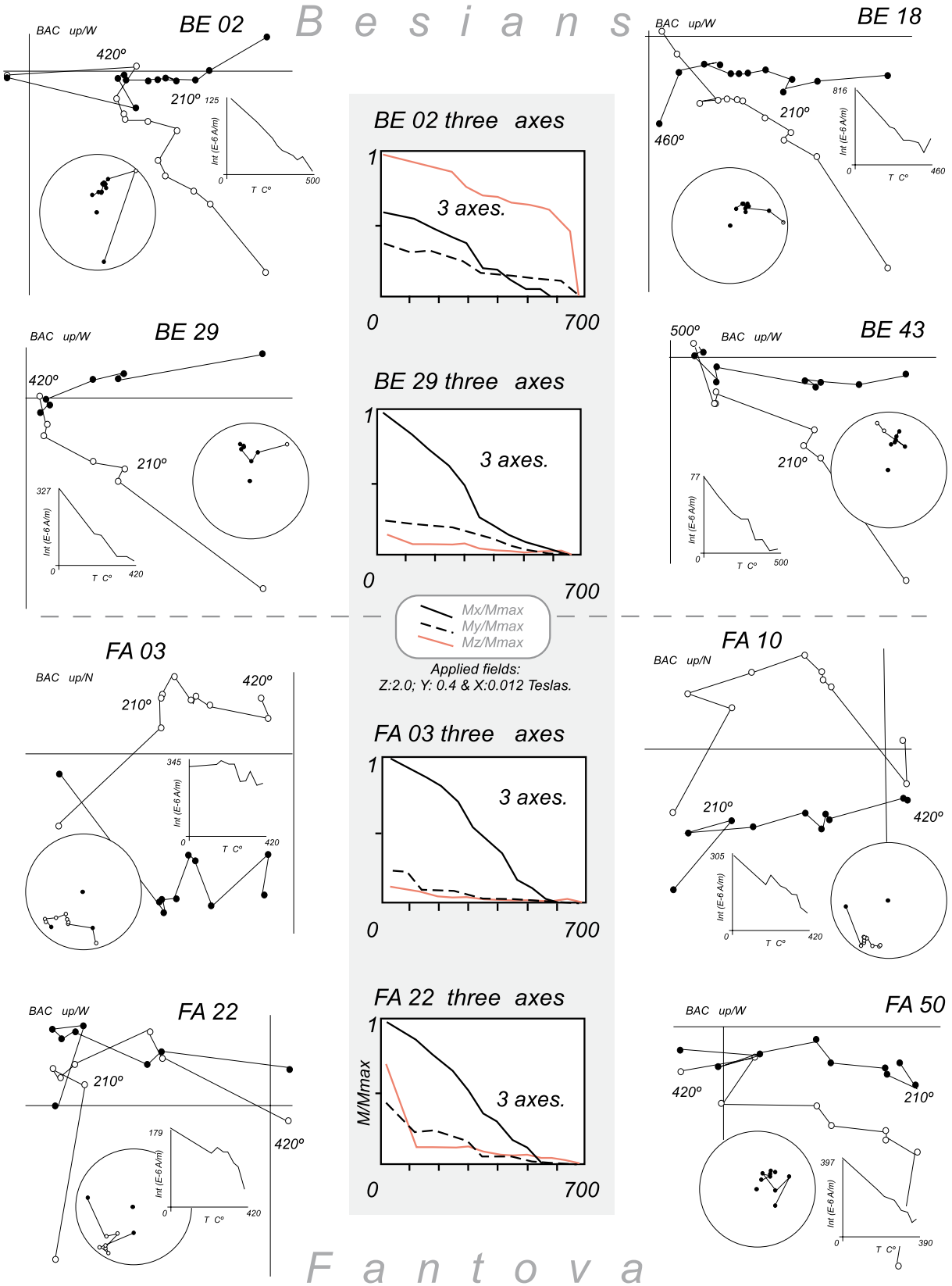

FIGURE 10. Rock magnetism analyses of 3 axes-IRM of representative samples at the central column (Lowrie's (1990) tests). Side columns are representative thermal demagnetization diagrams Before Any Correction (BAC, that is, geographic coordinate system). The stereographic projection and the intensity decay diagram are also included. Zijderveld's (1967) diagrams.

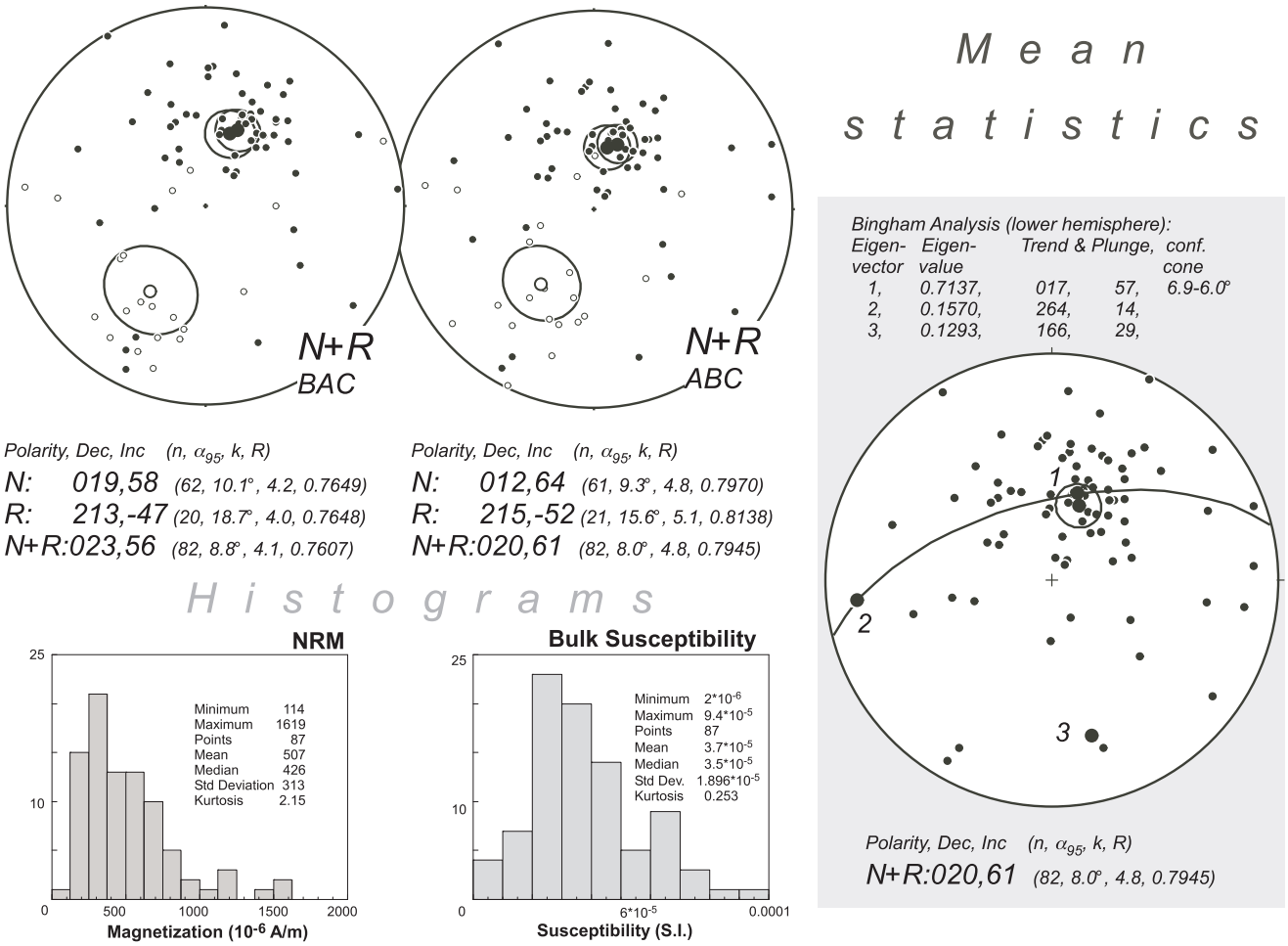

FIGURE 11. Mean statistics of the dataset by polarity (left plots) Before Any Correction (BAC) and After Bedding Correction (ABC); and all together at the lower hemisphere (right stereoplot). Natural Remanent Magnetization (NRM) (left) and bulk susceptibility histograms (right) are also shown at the lower-left side.

INTERPRETATION AND DISCUSSION

Biostratigraphy

In the Puebla de Fantova section (Fig. 4), the foraminiferal assemblage composed of *N. quasilaevigatus*, *N. britannicus*, *N. praediscorbinus*, *N. campesinus*, *N. friulanus*, *N. praelorioli*, *N. manfredi* and *Assilina maior* indicates a late Ypresian (late Cuisian) age (Biozone Nummulites manfredi according to Schaub, 1981). In the same stratigraphic section, the assemblage formed by *Alveolina violae* and *Alveolina pinguis* also indicates a late Ypresian (late Cuisian) age (Biozone Alveolina violae according to Hottinger (1960, 1974) and Hottinger and Drobne (1988)). Both biozones are equivalent to SBZ 12 of Serra-Kiel *et al.* (1998).

In the Besians section (Fig. 5), sample B 1 yielded an assemblage composed of *N. quasilaevigatus*, *N. manfredi* and *N. campesinus*, that according to Schaub (1981) indicates a late Ypresian (late Cuisian) age (Biozone Nummulites manfredi), equivalent to SBZ 12 of Serra-Kiel *et al.* (1998). The samples B 2-B 7 contain an assemblage of *N. praelorioli*, *N. laevigatus*, *N. gallensis*, *N. lehneri*, *N. messinae*, *Assilina tenuimarginata* and *Assilina spira abrardi*, that indicate a Lutetian age according to Schaub (1981) (Biozone Nummulites laevigatus), equivalent to SBZ 13 of Serra-Kiel *et al.* (1998).

In the samples from La Puebla de Fantova section (Fig. 4; Table 1), markers of calcareous nannofossil zones are almost absent due to the poor fossil preservation; therefore, the assignment to a specific zone has been done with auxiliary markers, so that the zonal assignment may not be accurate.

The dominance in the autochthonous assemblage of *Reticulofenestra*, together with the presence of *C. crassus* and the absence of *Tribrachiatus orthostylus* and *D. sublodoensis* pointed that the first 9 samples of the Puebla

TABLE 2. Mean paleomagnetic data in the studied profiles; La Puebla de Fantova, Besians and all data merged together. DEC= declination and INC= inclination in-situ Before Any Correction (BAC) and restored After Bedding Correction (ABC) together with standard statistical parameters (N= number of data, $\alpha 95$= confidence angle, *k* concentration parameter and R= unitary vector)

		Insitu (BAC)						Restored (ABC)					
		N	DEC	INC	α_{95}	*k*	R	N	DEC	INC	α_{95}	*k*	R
La Puebla de Fantova	N	29	357.0	68.0	-	-	0.6004	27	349.4	70.1	20.3	5.1	0.6637
	R	19	256.1	-44.9	15.6	5.6	0.8313	21	215.3	-51.9	15.6	5.1	0.8138
	N+R	48	021.9	58.5	14.7	2.9	0.6673	48	018.8	63.0	12.3	3.4	0.7083
Besians	N	33	026.3	52.0	6.8	14.4	0.9329	34	020.7	59.3	7.5	11.7	0.9172
	R	1	-	-	-	-	-	0	-	-	-	-	-
	N+R	34	024.2	53.1	9.2	0.8948	0.8948	34	020.7	59.3	7.5	11.7	0.9172
Fantova + Besians	N	62	018.9	58.4	4.2	0.7649	0.7649	61	012.1	63.9	9.3	4.8	0.7970
	R	20	213.0	-47,3	4.0	0.7648	0.7648	21	215.3	-51.9	15.6	5.1	0.8138
	N+R	82	023.1	-55.9	4.1	0.7607	0.7607	82	019.7	61.2	8.0	4.8	0.7945

de Fantova section pertain to zone NP13. Sample F 10n, located in the middle part of the section, registered the presence of *Discoaster sublodoensis*, the marker species of the base of zone NP14. This means that at least the upper 150m of the Puebla de Fantova section belongs to zone NP14 (CP12a). Sample F 13n, located in the uppermost part of the section, is stratigraphically equivalent to sample 24 of the Campo section (Santa Liestra tunnel) described by Kapellos and Schaub (1973). According to these authors, sample 24 belongs to zone NP14 (CP12a). However, we must highlight that all the attempts to reproduce the results reported by Kapellos and Schaub (1973) for samples 23-24 of the Campo section were unsuccessful. The samples collected near the Santa Liestra tunnel showed only reworked Cretaceous specimens or were barren.

The calcareous nannofossil assemblages recorded in the Besians section (Fig. 5; Table 1) are not good enough to assign them to a specific zone. Sample B 2n is stratigrafically equivalent to samples 102-105 of the Campo section (Perarrúa) studied by Kapellos and Schaub (1973). These authors pointed out that these samples contained, among other species, *Chiphragmalithus* aff. *quadratus*. But, the specimen depicted by these authors in their plate 7, fig. 15, is closer to *Nannotetrina cristata*, which first occurrence is slightly preceded by the first occurrence of *Blackites inflatus*, the marker species of subzone CP12b (Agnini *et al.*, 2014; Bernaola *et al.*, 2006; Tori and Monechi, 2013; Westerhold *et al.*, 2017). Therefore, the upper part of the Besians section could be assigned to subzone CP12b.

Magnetic local polarity sequence and correlation

We have calculated the VGPs from the ChRMs after bedding restoration along the studied profiles (only type 1 and 2 samples were used for such purpose). The VGP latitude log has allowed building the LPS for each profile; La Puebla de Fantova (Fig. 12) and Besians (Fig. 13). At La Puebla de Fantova section, from bottom to top, we can identify a reverse and a normal polarity magnetozones; R1 and N1. Magnetozones R1 and N1 are built with 8 and 18 sites respectively and expand along the section from the base to meter 58 (R1) and then up to meter 162 (N1). At Besians section (Fig. 13), all the samples display normal polarity, as it was identified in 47 different stratigraphic levels (90% of type 1-catalogued quality). This relatively simple pattern of magnetozones is robust and clear, even in magnetozone R1 (La Puebla de Fantova section) that is characterized by more than 20 consecutive levels where reverse polarity was identified.

The sampling was initially designed to avoid any possible stratigraphic gap between the two sampled sections and thus we used the sharp transition between the cartographic units 23 and 24 of Teixell *et al.* (2016) as the correlation level; the correlation follows the lowest first prominent coarse levels located at the top of La Puebla de Fantova section (about meter 220), to the equivalent levels at the Besians section (about meter 30 from the base) (Fig. 14) in the same stratigraphic unit. As a whole (Fig. 14), only two magnetozones are found. The lower part of the Puebla de Fantova section shows reverse polarity (R1 magnetozone) whereas the rest of the Puebla de Fantova and the Besians sections show a normal polarity signal (N1).

Data integration and interpretation

The correlation between the Puebla de Fantova and Besians sections (Fig. 14) allows clarifying the chronostratigraphy along the Ésera valley section, which includes the Y/L boundary. The Puebla de Fantova section (Figs. 3; 4; 12; 14) is above the lower Ésera section (Navarri section of Bentham and Burbank, 1996, or Morillo de Liena section of Payros *et al.*, 2009b), with an interval unsampled for paleomagnetism in-between, which corresponds to the Lower Campanúe conglomerate (Santa Liestra-1; Fig. 2), as explained above. The lower Ésera section ends, in terms of paleomagnetic data (Bentham and Burbank, 1996), at the base of Lower Campanúe conglomerates (BB-1 in Fig. 3). The Lower Pararrúa

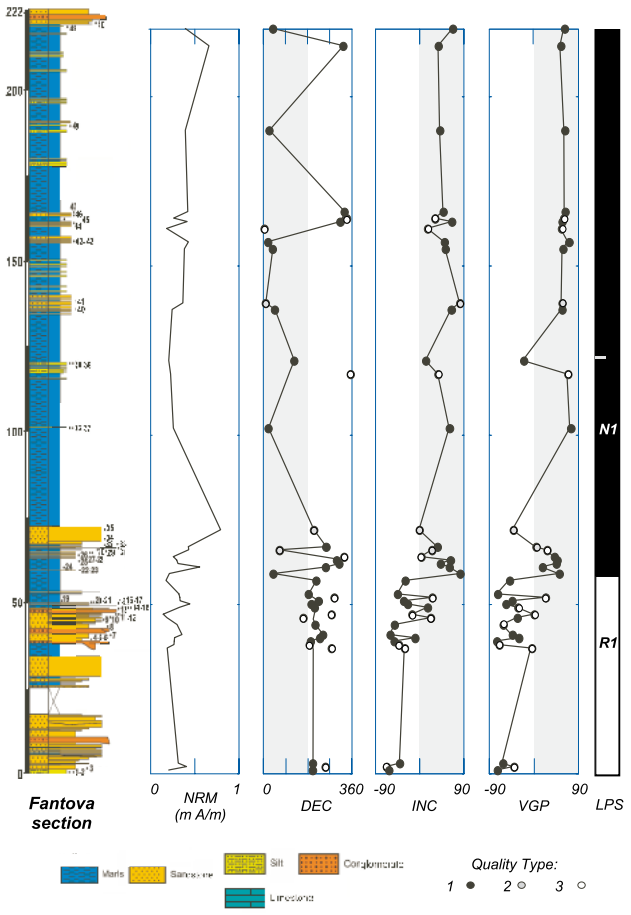

FIGURE 12. La Puebla de Fantova section magnetostratigraphic results. From left to right: Detailed stratigraphic column, Natural Remanent Magnetization (NRM) log (intensity in mA/m). Declination and inclination (DEC and INC) logs after bedding correction. Determined Virtual Geomagnetic Poles (VGP) paleolatitude log and the final Local Polarity Sequence (LPS). Stratigraphic key and paleomagnetic types in Figure 13.

marls (Fig. 2), below this conglomerate, contain SBZ 11 (middle Cuisian) larger foraminifera (Kapellos and Schaub, 1973; Schaub, 1981; Tosquella, 1995), calcareous nannofossils of the NP13 to NP14 transition (Payros *et al.*, 2009b following data of Kapellos and Schaub, 1973) and include the uppermost C22r, the entire C22n, and the base of C21r (Bentham and Burbank, 1996). The upper limit of C21r in the Ésera valley section was unsolved. The Santa Liestra section (Bentham and Burbank, 1996; Payros *et al.*, 2009b) (BB-2 in Fig. 3), which follows the Navarri section, starts in normal polarity magnetic values with an unsampled intermediate stratigraphic gap. The Santa Liestra section is lateral-equivalent to the upper part of the Puebla de Fantova section and the lower part of the Besians section (Figs. 5; 13) showing normal polarity. After the data and results presented in this study, only the Lower Campanúe conglomerates remains partially un-sampled for magnetostratigraphy.

According to Speijer *et al.* (2020), the NP13/NP14 boundary appears near the C22n/C21r transition, in the upper part of SBZ 11, in agreement with its occurrence in the Lower Perarrua unit (Payros *et al.*, 2009b). The lower reverse magnetic polarity (R1), found in the Puebla de Fantova section (Fig. 14), which contains SBZ 12 larger foraminifera, is interpreted as belonging to C21r. The inverse/normal polarity boundary, which occurs in the lower part of this section, is interpreted as the C21r/C21n boundary. The rest of the Puebla de Fantova and the complete Besians sections (Figs. 3; 5; 13; 14), with a normal-polarity signal (N1), are interpreted as C21n (Fig. 14). Below the correlation point between the Puebla de Fantova and Besians sections, C21n contains SBZ 12 larger foraminifera and NP14 (CP12a) calcareous nannofossils. Above the correlation point, after a stretch without fossil data, it contains SBZ 13 larger foraminifera and CP12b calcareous nannofossil forms in the upper part of the Besians section (Figs. 5; 14).

Discussion

The scarcity and poor preservation of calcareous nannofossils precluded the possibility of fixing a precise location for the Ypresian/Lutetian boundary in the Ésera valley section. Nevertheless, the existing data (from samples in this study and previous works: Kapellos and Schaub, 1973; Payros *et al.*, 2009b) is enough to confirm the robustness of the interpretation, despite the calcareous nannofossil zone markers appear in a younger stratigraphic position than expected.

In the Puebla de Fantova section, the FO of *D. sublodoensis*, the marker of the base of zone NP14 (CP12a), is registered in sample F 10n, with normal polarity (C21n) and SBZ12 larger foraminifera. One of the two *D. sublodoensis* specimens found in this sample was a 5-rayed *D. sublodoensis* (Table 1) that according to Agnini *et al.* (2014) its First Common Occurrence (FCO) is at the base of chon C21r, slightly after the FO of rare *D. sublodoensis* in chron C22n.

Thus, the finding of two specimens of *D. sublodoensis* in sample F 10n confirms the attribution to chon C21n of the normal polarity signal N1 and suggests that the absence of zone NP14 (P12a) marker species at the base of the Puebla de Fantova section is due to poor preservation of the calcareous nannofossil assemblages in this section.

The base of the Subzone CP12b is recorded by stratigraphic correlation in the lower third of the Besians section and is given by the FO of *N. cristata* in samples CK 102-105 in the Campo (Perarrúa) section (Kapellos and Schaub, 1973). In their work, these authors provide a list of species present for a given range of samples but

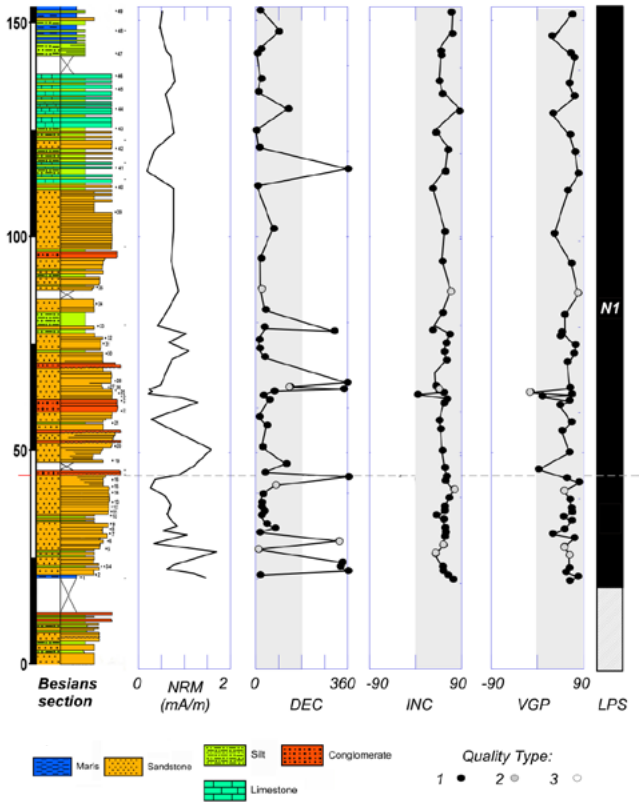

FIGURE 13. Besians section magnetostratigraphic results (see Figure 12 caption).

do not detail the association of calcareous nannofossils for each of the studied samples. This prevents us from knowing if some of the studied samples had very poor preserved calcareous nannofossil assemblages or even if calcareous nannofossils were absent in some of the samples. Several attempts to reproduce the results obtained by Kapellos and Schaub (1973) in the samples CK 23-24 from the Campo section (equivalent to F13n) have shown that the calcareous nannofossil assemblages of these samples are exclusively composed of reworked Cretaceous species or even that in some of the samples calcareous nannofossils are absent.

The above observations suggest that the absence of subzone CP12b markers in CK19-25 samples at Campo section and in the upper half of the Puebla de Fantova section is due to the poor preservation of calcareous nannofossil assemblages.

The obtained larger foraminifera distribution is in agreement with published data (Payros *et al.*, 2009b; Schaub, 1966, 1973, 1981, 1992; Tosquella, 1995; Tosquella and Serra-Kiel, 1998). However, when contrasted with the magnetic polarity zones, some degree of conflict with previously standardized chronostratigraphic charts for this stratigraphic interval (Luterbacher *et al.*, 2005; Serra-Kiel *et al.*, 1998; Speijer *et al.*, 2020) appears (Fig. 15).

Recent works (Speijer *et al.*, 2020), based on data correlation between larger foraminifera, with calcareous nannofossils and magnetostratigraphy from the South Pyrenean Basin (Costa *et al.*, 2013; Molina *et al.*, 2003; Payros *et al.*, 2009b; Pujalte *et al.*, 2009; Rodríguez-Pintó *et al.*, 2012, 2013; Schneider and Speijer, 2009) slightly modified the boundaries between SBZs of previous authors (Luterbacher *et al.*, 2005; Serra-Kiel *et al.*, 1998). Boundaries between the SBZs always kept some degree of uncertainty because they were based on fossil associations (assemblage zones) of organisms closely linked to ecological parameters (stenobionts) thus making difficult their precise calibration (Hallock, 1985, 1999; Hohenegger *et al.*, 1999; Langer and Hottinger, 2000; Oron *et al.*, 2018; Renema and Troelstra, 2001). In particular, the SBZ 12 to SBZ 13 boundary was estimated tentatively around the Y/L boundary whithin C21r (Speijer *et al.*, 2020). Data from western Pyrenees (Gorrondatxe and Otsakar sections) (Molina *et al.*, 2011; Orue-Etxebarria *et al.*, 2006; Payros *et al.*, 2007, 2011), only provide shelf derived larger foraminifera in resedimented beds, with a significant lack of larger foraminiferal data toward the Y/L transition. In the shallow carbonate platform and slope transitions of the South Pyrenean foreland margin (San Pelegrin and Ainsa Basin around the Boltaña anticline) (Mochales *et al.*, 2012; Rodríguez-Pintó *et al.*, 2013), as well as in the Gabardiella section to the West (Rodríguez-Pintó *et al.*, 2017), the Y/L transition is hampered by stratigraphic gaps. Conversely, the Ésera valley section displays a thick shallow marine succession that includes the Ypresian/Lutetian transition, rich in larger foraminifera (Payros *et al.*, 2009b; Schaub, 1966, 1973, 1981, 1992; Tosquella, 1995; Tosquella and Serra-Kiel, 1998).

Outside of the Pyrenees, the Agost section (Betic Chain, western Tethys) provides a chronostratigraphic dataset including calcareous nanofossils, larger foraminifera and magnetic polarity (Larrasoaña *et al.*, 2008). In the Agost section, larger foraminifera also appear as reworked components outside their original habitat, with apparent no mixture of different age specimens (Larrasoaña *et al.*, 2008). Larger foraminifera found around the CP12a/CP12b boundary (Y/L boundary), within C21r, still belong to the SBZ 11 (Larrasoaña *et al.*, 2008). The SBZ 12 and SBZ 13 forms are found in C21n. In the Agost section, larger foraminifera forms appear in a younger stratigraphic position than in the Ésera valley, which expects to reworked faunas.

With the obtained magnetic polarity dataset for the Y/L transition, data from the shallow marine Ésera valley sections (La Puebla de Fantova and Besians) results in a robust stratigraphic chart for the larger foraminifera distribution around the C21. These results allow shifting the SBZ 12-SBZ 13 boundary to the lower part of C21n

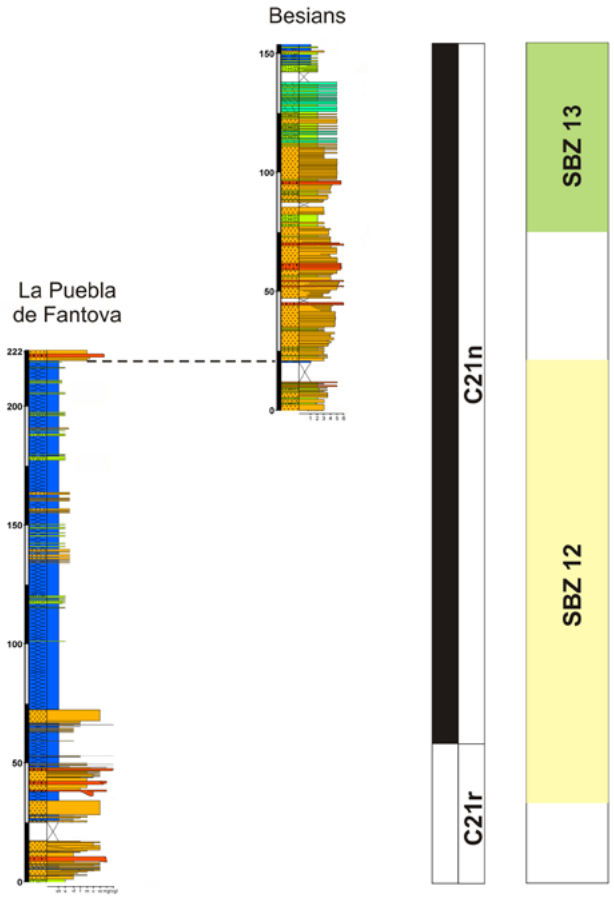

FIGURE 14. La Puebla de Fantova and Besians sections: Correlation and stratigraphic interpretation. Stratigraphic key as in Figure 13.

(Fig. 15). Accordingly, the Y/L boundary occurs within SBZ 12.

CONCLUSIONS

The larger foraminiferal assemblages found in the Puebla de Fantova section and in the lowest sample (B1) of the Besians section belong to the Nummulites manfredi Biozone (Schaub, 1981) and the Alveolina violae Biozone (Hottinger, 1960, 1974; Hottinger and Drobne, 1988), which are equivalent to SBZ 12 of Serra-Kiel *et al.* (1998). The rest of samples from the Besians section yielded larger foraminiferal assemblages belonging to the Nummulites laevigatus Biozone (Schaub, 1981), equivalent to SBZ 13 of Serra-Kiel *et al.* (1998).

The calcareous nannofossil assemblages are very poorly preserved and showed low abundance of autochthonous specimens. According to these assemblages the lower half of La Puebla de Fantova section belongs to Zone NP13 (CP11), and the upper half of this section and the lower part of the Besians section belong to Zone NP14 (CP12a). The rest of the Besians section belongs to Zone NP14 (CP12b). However, due to the poor preservation of the assemblages, the zone markers are almost absent and thus their first occurrences in the studied sections occur in a younger position than expected.

A robust local polarity sequence was built and based on 87 reliable paleomagnetic determinations in the two studied sections (La Puebla de Fantova and Besians) with

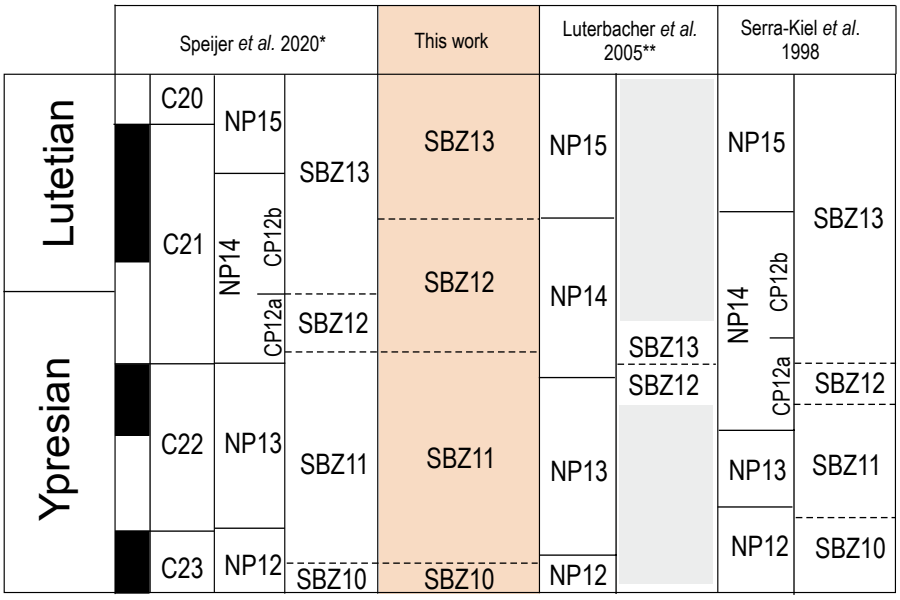

FIGURE 15. Proposal of a new time scale for the Ypresian/Lutetian transition including magnetic geochronology, calcareous nannofossils and larger benthic foraminiferal zones, after Serra-Kiel *et al.* (1998); Luterbacher *et al.* (2005) and Speijer *et al.* (2020) compared with the larger benthic foraminiferal zonation after this work.

an unambiguous stratigraphic correlation. Characteristic directions are pseudo-antiparallel and considered as a primary record of the magnetic field supported by several paleomagnetic studies in the region. Two local chrons (R1, N1) together with the biostratigraphic information (larger foraminifera and calcareous nannofossils) allow us proposing a new age model for the Ésera valley section, the most complete section in the Southern Pyrenees across the Y/L transition. There, the SBZ 12 faunal assemblages, identified since now as late Cuisian (uppermost Ypresian) (Speijer *et al.*, 2020 and references herein), extend across the Y/L boundary, ranging into the lower part of C21n.

ACKNOWLEDGMENTS

AB fieldwork has been supported by the project PGC2018-093903-C1, additional support came from the projects DR3AM (CGL2014-54118-C2-2-R) MAGIBER-II (CGL2017-90632-REDT) and UKRIA4D (PID2019-104693GB-I00/CTA) all of them from the Spanish Science National Plan. The study of calcareous nannofossils was supported by the Research Group of the Basque University System IT-1602-22. Pablo Calvín gave us a hand with the reversal test in Python. The accurate and constructive comments from Johannes Pignatti, Elisabet Beamud, the Journal Manager Laura Rincón, and the editors Carles Martín Closas, Eulàlia Gili and Miguel Garcés helped to improve the original manuscript.

REFERENCES

Agnini, C., Muttoni, G., Kent, D.V., Rio, D., 2006. Eocene biostratigraphy and magnetic stratigraphy from Possagno, Italy: the calcareous nannofossil response to climatic variability. Earth and Planetary Science Letters, 241, 815-830.

Agnini, C., Fornaciari, E., Raffi, I., Catanzariti, R., Pälike, H., Backman, J., Rio, D., 2014. Biozonation and biochronology of Paleogene calcareous nannofossils from low and middle latitudes. Newsletters on Stratigraphy, 47, 131-181. DOI: http://doi.org/10.1127/0078□0421/2014/0042

Allmendinger, R.W., Cardozo, N.C., Fisher, D., 2013. Structural geology algorithms: Vectors & Tensors. Cambridge, Cambridge University Press, 289pp.

Atkinson, C.D., 1986. Tectonic control on alluvial sedimentation as revealed by an ancient catena in the Capella Formation (Eocene) of Northern Spain. In: Wright, V.P. (ed.). Palaeosols: their Recognition and Interpretation. Oxford, Blackwells, 139-179.

Atkinson, C.D., Elliott, K.T., 1985. Patterns of sedimentation in the South Pyrenean Basin: a tectono-sedimentary model for molasse accumulation in a thrust sheet top basin. In: Allen, P.A.A., Homewood, P., Williams, G.D. (eds.). Abstracts of the International symposium on Foreland basins. Fribourg (Switzerland), International Association of Sedimentologists Thematic meeting, 32.

Aubry, M.P., 1995. From chronology to stratigraphy: interpreting the Lower and Middle Eocene stratigraphic record in the Atlantic Ocean. In: Berggren, W.A., Kent, D.V., Aubry, M.P., Hardenbol, J. (eds.). Geochronology, Time Scales and Global Stratigraphic Correlation. Society for Sedimentary Geology (SEPM) Special Publication, 54, 213-274.

Backman, J., 1986. Late Paleocene to middle Eocene calcareous nannofossil biochronology from Shatsky Rise, Walvis Ridge and Italy. Palaeogeography, Palaeoclimatology, Palaeoecology, 57, 43-59.

Barnolas, A., Pujalte, V., 2004. La Cordillera Pirenaica. Definición, límites y división. In: Vera, J.A. (ed.). Geología de España. Instituto Geológico y Minero de España, Sociedad Geológica de España, 233-241.

Barnolas, A., Samsó, J.M., Teixell, A., Tosquella, J., Zamorano, M., 1991. Evolución sedimentaria entre la cuenca de Graus-Tremp y la cuenca de Jaca-Pamplona. In: Colombo, F. (ed.). Libro-Guía Excursión 1. I Congreso del Grupo Español del Terciario. Vic (Spain), EUMO Gràfic, 123pp.

Barnolas, A., Payros, A., Samsó, J.M., 2004. La Cuenca surpirenaica desde el Ilerdiense medio al Priaboniense. In: Vera, J.A. (ed.). Geología de España. Instituto Geológico y Minero de España, Sociedad Geológica de España, 313-320.

Barnolas, A., Larrasoaña, J.C., Pujalte, V., Schmitz, B., Sierro, F.J., Mata, M.P., van der Berg, B.C.J., Pérez-Asensio, J.N., Salazar, A., Salvany, J.M., Ledesma, S., García-Castellanos, D., Civis, J., Cunha, P., 2019. Alpine Foreland Basins. In: Quesada, C., Oliveira, J.T. (eds.). The Geology of Iberia: A Geodynamic Approach. Springer Nature, 4, 7-59.

Beamud, E., Garcés, M., Muñoz, J.A., Cabrera, Ll., Almar, Y., 2004. Distribución de las rotaciones paleomagnéticas en la cuenca de Graus-Tremp durante el Terciario. Geotemas, 6(4), 283-285.

Bentham, P., Burbank, D.W., 1996. Chronology of Eocene foreland basin evolution along the western oblique margin of the South-Central Pyrenees. In: Friend, P.F., Dabrio, C.J. (eds.). Tertiary basins of Spain. Cambridge, Cambridge University Press, 144-152.

Bernaola, G., Orue-Etxebarria, X., Payros, A., Dinarès-Turell, J., Tosquella, J., Apellaniz, E., Caballero, F., 2006. Biomagnetostratigraphic analysis of the Gorrondatxe section (Basque Country, Western Pyrenees): Its significance for the definition of the Ypresian/Lutetian boundary stratotype. Neues Jahrbuch für Geologie und Paläontologie Abhandlungen, 241, 67-109.

Bingham, C., 1974. An antipodally symmetric distribution on the sphere. The Annals of Statistics, 2(6), 1201-1225.

de Boer, P.L., Pragt, J.S.J., Oost, A.P., 1991. Vertically persistent sedimentary facies boundaries along growth anticlines and climate-controlled sedimentation in the thrust-sheet-top South Pyrenean Tremp-Graus Foreland Basin. Basin Research, 3(2), 63-78.

Bown, P.R., 2005. Paleogene calcareous nannofossils from the Kilwa and Lindi areas of coastal Tanzania: Tanzania Drilling Project Sites 1 to 10. Journal of Nannoplankton Research, 27, 21-95.

Bown, P.R., Young, J.R., 1998. Techniques. In: Bown, P.R. (ed.). Calcareous Nannofossil Biostratigraphy. British Micropaleontological Society Publications Series, London, Kluwer Academic Press, 16-28.

Cardozo, N., Allmendinger, R.W., 2013. Spherical projections with OSXStereonet. Computers & Geosciences, 51(0), 193-205.

Chanvry, E., Deschamps, R., Joseph, Ph., Puigdefàbregas, C., Poyatos-Moré, M., Serra-Kiel, J., Garcia, D., Teinturier, S., 2018. The influence of intrabasinal tectonics in the stratigraphic evolution of piggyback basin fills: Towards a model from the Tremp-Graus-Ainsa Basin (South-Pyrenean Zone, Spain). Sedimentary Geology, 377, 34-62.

Costa, E., Garcés, M., López-Blanco, M., Serra-Kiel, J., Bernaola, G., Cabrera, L., Beamud, E., 2013. The Bartonian–Priabonian marine record of the eastern South Pyrenean foreland basin (NE Spain): a new calibration of the larger foraminifers and calcareous nannofossil biozonation. Geologica Acta, 11(2), 177-193. DOI: http://dx.doi.org/10.1344/105.000001779

Crumeyrolle, Ph., 1987. Stratigraphie physique et sédimetation des systèmes de dépôt de la séquence de Santa Liestra (Eocéne sud-pyrénéen, Pyrénées Aragonaises, Espagne). Thèse. Université de Bordeaux III, unpublished, 216pp.

Crumeyrolle, P., Mutti, E., 1986. Stratigraphy and sedimentology of Santa Liestra shelf depositional systems; South-Pyrenean Eocene basin, Province of Huesca, Spain. Comptes Rendus de l'Académie des Sciences, Serie, 2(7), 581-584.

Cuevas-Gozalo, M.C., 1989. Sedimentary facies and sequential architecture of tide-influenced alluvial deposits. Geologica Ultraiectina, 61, 152pp.

Dinarès-Turell, J., 1992. Paleomagnetisme a les unitats sudpirinenques superiors. Implicacions estructurals. PhD Thesis. Barcelona (Spain), Universitat de Barcelona, unpublished, 462pp.

van Eden, J.G., 1970. A reconnaissance of deltaic environment in the Middle Eocene of the South-Central Pyrenees, Spain. Geologie en Mijnbouw, 49(2), 145-157.

Fisher, R.A., 1953. Dispersion on a sphere. Proceedings of the Royal Society A, 217, 295-305.

Garcés, M., López-Blanco, M., Valero, L., Beamud, E., Muñoz, J.A., Oliva-Urcía, B., Vinyoles, A., Arbués, P., Cabello, P., Cabrera, Ll., 2020. Paleogeographic and sedimentary evolution of the South-Pyrenean foreland basin. Marine and Petroleum Geology, 113, 104105. DOI: https://doi.org/10.1016/j.marpetgeo.2019.104105

Garrido-Mejías, A., 1968. Sobre la estratigrafía de los conglomerados de Campanué (Santa Liestra) y formaciones superiores del Eoceno (extremo occidental de la Cuenca Tremp-Graus, Pirineo Central, provincia de Huesca. Acta Geologica Hispanica, 3(2), 39-43.

Hallock, P., 1985. Why are larger foraminifera large? Paleobiology, 11, 195-208.

Hallock, P., 1999. Symbiont-bearing foraminifera. In: Gupta, B.K.S. (ed.). Modern Foraminifera. Amsterdam, Kluwer Academic, 123-139.

Hohenegger, J., Yordanova, E., Nakano, Y., Tatzreiter, F., 1999. Habitats of larger foraminifera on the upper reef slope of Sesoko Island, Okinawa, Japan. Marine Micropaleontology, 36, 109-168.

Honegger, L., Adatte, T., Spangenberg, J.E., Rugenstein, J.K.C., Poyatos-Moré, M., Puigdefàbregas, C., Chanvry, E., Clark, J., Fildani, A., Verrechia, E., Kouzmanov, K., Harlaux, M., Castelltort, S., 2020. Alluvial record of an early Eocene hyperthermal within the Castissent Formation, the Pyrenees, Spain. Climate of the Past, 16, 227-243.

Hottinger, L., 1960. Recherches sur les Alvéolines du Paléocène et de l'Eocène. Mémoires suisses de paléontologie, 75/76, 243pp.

Hottinger, L., 1974. Alveolinids, Cretaceous-Tertiary. Larger Foraminifera. Esso Production Research-European Laboratories, A. Schudel & Co. AG. Riehen/Basle, 84pp, 106pls.

Hottinger, L., Drobne, K., 1988. Alveolines tertiaires: quelques problèmes liés à la conception de l'espèce. Revue de Paléobiologie, 2 (Volume Spéciale), 665-681.

Hottinger, L., Schaub, H., 1964. Le synchronisme des biozones basé sur les Nummulites, Assilines et Alveolines. Mémoires Bureau Recherche Géologique et Minière, 28, 625-629.

Kapellos, Ch., Schaub, H., 1973. Zur Korrelation von Biozonierungen mit Grossforaminiferen und Nannoplakton im Paläogen der Pyrenäen. Eclogae geologicae Helvetiae, 66(3), 687-737.

Kirschvink, J.L., 1980. The least-squares line and plane and the analysis of paleomagnetic data. Geophysical Journal of the Royal Astronomical Society, 62, 699-718.

Langer, M.R., Hottinger, L.C., 2000. Biogeography of selected `larger' foraminifera. Micropaleontology, 46, 105-127.

Larrasoaña, J.C., Parés, J.C., Pueyo, E.L., 2003. Stable Eocene magnetization carried by magnetite and magnetic iron sulphides in marine marls (Pamplona-Arguis Formation, southern Pyrenees, N Spain). Studia Geophysica Geodetica, 47, 237-254.

Larrasoaña, J.C., Gonzalvo, C., Molina, E., Monechi, S., Ortiz, S., Tori, F., Tosquella, J., 2008. Integrated magnetobiochronology of the Early/Midlle Eocene transition at Agost (Spain): Implications for defining the Ypresian/Lutetian boundary stratotype. Lethaia, 41, 395-415.

López-Olmedo, F., Ardèvol, L., 2016. Hoja nº 251 (Aren) del Mapa geológico de España a escala 1:50.000 (MAGNA). Madrid, Instituto Geológico y Minero de España (IGME).

Lowrie, W., 1990. Identification of ferromagnetic minerals in a rock by coercitivity and unblocking temperature properties. Geophysical Research Letters, 17(2), 159-162.

Luterbacher, H., Ali, J., Brinkhuis, H., Gradstein, F., Hooker, J., Monechi, S., Ogg, J., Powell, J., Röhl, U., Sanfilippo, A., 2005. The Paleogene period. In: Gradstein, F.M., Ogg, J.G., Smith, A.G. (eds.). A Geologic Time Scale 2004. Cambridge (U.K.), Cambridge University Press, 384-408.

Martini, E., 1971. Standard Tertiary and Quaternary calcareous nannoplankton zonation. In: Farinacci, A. (ed.). Proceedings of the Second International Conference of Planktonic Microfossils. Edizioni Tecnoscienza, 2, 739-785.

Mochales, T., Barnolas, A., Pueyo, E.L., Casas, A.M., Serra-Kiel, J., Samsó, J.M., Ramajo, J., Sanjuán, J., 2012. Chronostratigraphy of the Boltaña anticline and the Ainsa Basin (Southern Pyrenees). Geological Society of America (GSA) Bulletin, 124(7-8), 1229-1250.

Molina, E., Angori, E., Arenillas, I., Brinkhuis, H., Crouch, E.M., Luterbacher, H., Monechi, S., Schmitz, B., 2003. Correlation between the Paleocene/Eocene boundary and the Ilerdian at Campo, Spain. Revue de Micropaléontologie, 46, 95-109.

Molina, E., Alegret, L., Apellaniz, E., Bernaola, G., Caballero, F., Dinarès-Turell, J., Hardenbol, J., Heilmann-Clausen, C., Larrasoaña, J.C., Luterbacher, H., Monechi, S., Ortiz, S., Orue-Etxebarria, X., Payros, A., Pujalte, V., Rodríguez-Tovar, F.J., Tori, F., Tosquella, J., Uchman, A., 2011. The Global Stratotype Section and Point (GSSP) for the base of the Lutetian Stage at the Gorrondatxe section, Spain. Episodes, 34(2), 86-108.

Muñoz, J.A., Beamud, E., Fernández, O., Arbués, P., Dinarès-Turell, J., Poblet, J., 2013. The Ainsa Fold and thrust oblique zone of the central Pyrenees: Kinematics of a curved contractional system from paleomagnetic and structural data. Tectonics, 32, 1142-1175.

Mutti, E., Remacha, E., Sgavetti, M., Rosell, J., Valloni, R., Zamorano, M., 1985. Stratigraphy and Facies Characteristics of the Eocene Hecho Group Turbidite Systems, South-Central Pyrenees. International Association of Sedimentologists, 6th. Europen Regional Meeting, Excursion Guidebook, 12, 519-576.

Mutti, E., Séguret, M. Sgavetti, M., 1988. Sedimentation and deformation in the Tertiary sequences of the southern Pyrenees. Nice, American Association of Petroleum Geologists (AAPG). Mediterranean Basins Conference and Exhibition, Field-Trip Guidebook, 7, 169pp.

Nijman, W., 1998. Cyclicity and basin axis shift in a piggyback basin: towards modelling of the Eocene Tremp-Ager Basin, South Pyrenees, Spain. The Geological Society of London, 134 (Special Publications), 135-162.

Nijman, W., Nio, S.D., 1975. The Eocene Montañana delta (Tremp-Graus Basin, provinces of Lérida and Huesca, Southern Pyrenees, N. Spain). In: Rosell, J., Puigdefabregas, C. (eds.). The sedimentary evolution of the Paleogene South Pyrenean Basin. Nice (France), IXth International Congress, International Association of Sedimentologists (IAS), Excursion Guidebook, 19, 56pp.

Nijman, W., Puigdefabregas, C., 1989. The Second Stage of the Foreland Basin. In: Marzo, M., Puigdefabregas, C. (eds.). Alluvial deposits of the successive foreland basin stages and their relation to the Pyrenean thrust sequences. Guidebook Series of the 4th International Conference on Fluvial Sedimentology, Publicacions del Servei Geològic de Catalunya, 30-62.

Norris, R.D., Wilson, P.A., Blum, P., and the Expedition 342, 2014. Proceedings. IODP, 342: college Station, TX (Integrated Ocean Drilling Program). DOI: 10.2204/iodp.proc.342.2014

Okada, H., Bukry, D., 1980. Supplementary modification and introduction of code numbers to the low latitude cocolith biostratigraphic zonation (Bukry 1973, 1975). Marine Micropaleontology, 5, 321-325.

Oliva-Urcia, B., Pueyo, E.L., 2019. Paleomagnetism in structural geology and tectonics. In: Mukherjee, S. (ed.). Teaching methodologies in structural geology and tectonics. Heidelberg, Springer, 55-121 (67pp). ISBN: 978-981-13-2781-0.1

Opdyke, M.D., Channell, J.E., 1996. Magnetic stratigraphy. Academic press, 64, 346pp.

Oron, S., Abramovich, S., Almogi-Labin, A., Woeger, J., Erez, J., 2018. Deep related adaptations in symbiotic bearing benthic foraminifera: New insights from a field experiment on Operculina ammonoides. Scientific reports, 8:9560. DOI: 10.1038/s41598-018-27838-8

Orue-Etxebarria, X., Payros, A., Bernaola, G., Dinarès-Turell, J., Tosquella, J., Apellaniz, E., Caballero, F., 2006. The Ypresian/Lutetian boundary at the Gorrondatxe beach section (Basque Country, W Pyrenees). Climate and Biota of the Early Paleogene. Bilbao, Mid Conference Field Excursion Guidebook, 36pp.

Orue-Etxebarria, X., Payros, A., Caballero, F., Molina, E., Apellaniz, E., Bernaola, G. (eds.), 2009. The Ypresian/Lutetian transition in the Gorrondatxe Beach (Getxo, Western Pyrenees): Review, recent advances and future prospects. Getxo, 25-27 september 2009, International Workshop on the Ypresian/Lutetian Boundary Stratotype, 215pp. ISBN: 978-84-692-44876

Payros, A., Orue-Etxebarria, X., Pujalte, V., 2006. Covarying sedimentary and biotic fluctuations in Lower-Middle Eocene Pyrenean deep-sea deposits: Palaeoenvironmental implications. Palaeogeography, Palaeoclimatology, Palaeoecology, 234(2-4), 258-276.

Payros, A., Bernaola, G., Orue-Etxebarria, X., Dinarès-Turell, J., Tosquella, J., Apellaniz, E., 2007. Reassessment of the Early–Middle Eocene biomagnetochronology based on evidence from the Gorrondatxe section (Basque Country, western Pyrenees). Lethaia, 40, 183-195.

Payros, A., Orue-Etxebarria, X., Bernaola, G., Apellaniz, E., Dinarès-Turell, J., Tosquella, J., Caballero, F., 2009a. Characterization and astronomically calibrated age of the first occurrence of Turborotalia frontosa in the Gorrondatxe section, a prospective Lutetian GSSP: implications for the Eocene time scale. Lethaia, 42, 255-264.

Payros, A., Tosquella, J., Bernaola, G., Dinarès-Turell, J., Orue-Etxebarria, X., Pujalte, V., 2009b. Filling the North European Early/Middle Eocene (Ypresian/Lutetian) boundary gap: Insights from the Pyrenean continental to deep-marine record. Palaeogeography, Palaeoclimatology, Palaeoecology, 280, 313-332.

Payros, A., Dinarès-Turell, J., Bernaola, G., Orue-Etxebarria, X., Apellaniz, E., Tosquella, J., 2011. On the age of the

Early/Middle Eocene boundary and other related events: cyclostratigraphic refinements from the Pyrenean Otsakar section and the Lutetian GSSP. Geological Magazine, 148, 442-460.

Perch-Nielsen, K., 1985. Cenozoic calcareous nannofossils. In: Bolli, H.M., Saunders, J.B., Perch-Nielsen, K. (eds.). Plankton Stratigraphy. Cambridge, Cambridge University Press, 427-554.

Pocovi, A., Pueyo Anchuela, Ó., Pueyo, E.L., Casas-Sainz, A.M., Román Berdiel, M.T., Gil Imaz, A., Ramajo Cordero, J., Mochales, T., García Lasanta, C., Izquierdo, E., Parés, J.M., Sánchez, E., Soto Marín, R., Oliván, C., Rodríguez Pintó, A., Oliva-Urcia, B., Villalaín, J.J., 2014. Magnetic fabrics in the Central-Western Pyrenees: an overview. In: Almqvist, B., Henry, B., Jackson, M., Werner, T., Lagroix, F. (eds.). ASM in deformed rocks a tribute to Graham J. Borradaile. Tectonophysics, 629, 303-318.

Poyatos-Moré, M., 2014. Physical Stratigraphy and Facies Analysis of the Castissent Tecto-Sedimentary Unit (South-Central Pyrenees, Spain). Ph.D. Thesis. Cerdanyola del Vallès, Universitat Autònoma de Barcelona, 282pp.

Pueyo, E.L., Millán, H., Pocovı, A., 2002. Rotation velocity of a thrust: a paleomagnetic study in the External Sierras (Southern Pyrenees). Sedimentary Geology, 146(1-2), 191-208.

Pueyo-Anchuela, Ó., Casas-Sainz, A.M., Pueyo, E.L., Pocoví-Juan, A., Gil-Imaz, A., 2013. Analysis of the ferromagnetic contribution to the susceptibility by low field and high field methods in sedimentary rocks of the Southern Pyrenees and Northern Ebro foreland basin (Spain). Terra Nova, 25(4), 307-314.

Pujalte, V., Baceta, J.I., Schmitz, B., Orue-Etxebarria, X., Payros, A., Bernaola, G., Apellaniz, E., Caballero, F., Robador, A., Serra-Kiel, J., Tosquella, J., 2009. Redefinition of the Ilerdian Stage (early Eocene). Geologica Acta, 7(1-2), 177-194.

Ramón, M.J., Pueyo, E.L., Oliva-Urcia, B., Larrasoaña, J.C., 2017. Virtual directions in paleomagnetism: A global and rapid approach to evaluate the NRM components. Frontiers in Earth Science, 5, 8. DOI: 10.3389/feart.2017.00008

Renema, W., Troelstra, S.R., 2001. Larger foraminifera distribution on a mesotrophic carbonate shelf in SW Sulawesi (Indonesia). Palaeogeography, Palaeoclimatology, Palaeoecology, 175, 125-146.

Robador, A., Zamorano, M., 2013. Hoja nº 212 (Campo) del Mapa geológico de España a escala 1:50.000 (MAGNA). Madrid, Instituto Geológico y Minero de España (IGME).

Rodríguez-Pintó, A., Pueyo, E.L., Serra-Kiel, J., Samsó, J.M., Barnolas, A., Pocoví, A., 2012. Lutetian magnetostratigraphic calibration of larger foraminifera zonation (SBZ) in the Southern Pyrenees: The Isuela Section. Palaeogeography, Palaeoclimatology, Palaeoecology, 333-334, 107-120.

Rodríguez-Pintó, A., Pueyo, E.L., Serra-Kiel, J., Barnolas, A., Samsó, J.M., Pocoví, A., 2013. The Ypresian–Lutetian boundary in the Southwestern Pyrenean Basin; magnetostratigraphy from the San Pelegrín section. Palaeogeography, Palaeoclimatology, Palaeoecology, 370, 13-29.

Rodríguez-Pintó, A., Sanchez, E., Barnolas, A., Serra-Kiel, P., Samsó, J.M., Mochales, T., Pueyo, E.L., Scholger, R., 2017. Magnetostratigraphic data from lower part of Gabardiella section: Early - Middle Eocene, Southern Pyrenees. MAGIBER (Comisión de Paleomagnetismo de la Sociedad Geológica de España), X Valle del Grío, Universidad de Zaragoza, 30-33. ISBN: 978-84-16723-40-9

Rumpff, D., de Boer, P.L., 1985. A canyon-like marl filled depression in the Eocene Perarrúa fan-delta complex, S. Pyrenees, Spain. 6th International Association of Sedimentologists, European Regional Meeting Abstracts, 661-663.

Samsó, J.M., 1988. Estudi sedimentològic i biostratigràfic de la Formació St Esteve del Mall (Eocè, Conca de Tremp-Graus). Tesi de Llicenciatura. Barcelona, Universitat de Barcelona, Facultat de Geologia, unpublished, 540pp.

Schaub, H., 1951. Stratigraphie und Paläontologie des Schlierenflysches. Abhandlungen der Schweizerischen Paläontologischen Gesellschaft, 68, 222pp.

Schaub, H., 1966. Ueber die Grossforaminiferen im Untereocaen von Campo Ober-Aragonien). Eclogae Geologicae Helvetiae, 59, 355-377.

Schaub, H., 1973. La sección de Campo (Prov. de Huesca). XIII Coloquio Europeo de Micropaleontología, España, Comisión Nacional de Geología – Empresa Nacional Adaro de Investigaciones Mineras Sociedad Anónima, Madrid, Imprenta Pablo López, 151-170.

Schaub, H., 1981. Nummulites et Assilines de la Téthys Paléogène. Taxinomie, phylogénese et biostratigraphie. Mémoires suisses de paléontologie, 104-105-106, 236pp, 97pl.

Schaub, H., 1992. The Campo section (NE Spain), a Tethyan parastratotype of the Cuisian. Neues Jahrbuch für Geologie und Paläontologie, Abhandlungen, 186, 63-70.

Schneider, C., Speijer, R.P., 2009. Recalibration of the Tethyan shallow-benthic zonation across the Paleocene-Eocene boundary: the Egyptian record. Geologica Acta, 7(1-2), 195-214.

Séguret, M., 1972. Étude tectonique des nappes et séries décollées de la partie centrale du versant sud des Pyrénées - Caractère synsédimentaire, rôle de la compression et de la gravité. Montpellier, Publications de l'Université des Sciences et Techniques du Languedoc, Série géologie structurale, 2, 155pp.

Serra-Kiel, J., Hottinger, L., Caus, E., Ferràndez, C., Jauhri, A.K., Less, G., Pavlovec, R., Pignatti, J., Samsó, J.M., Schaub, H., Sirel, E., Strougo, A., Tosquella, J., Zakrevskaya, E., 1998. Larger foraminiferal biostratigraphy of the Tethyan Paleocene and Eocene. Bulletin de la Société géologique de France, 169(2), 281-299.

Speijer, R.P., Pälike, H., Hollis, C.J., Hooker, J.J., Ogg, J.G., 2020. The Paleogene Period (GTS 2020). In: Gradstein, F.M., Ogg, J.G., Schmitz, M.D., Ogg, G.M. (eds.). Geologic Time Scale 2020. Amsterdam, Elsevier, 2, 1087-1140. DOI: 10.1016/B978-0-12-824360-2.00028-0

Teixell, A., Zamorano, M., Ramírez, J.I., 2016. Hoja nº 250 (Graus) del Mapa geológico de España a escala 1:50.000 (MAGNA). Madrid, Instituto Geológico y Minero de España (IGME).

Tori, F., Monechi, S., 2013. Lutetian calcareous nannofossil events in the Agost section (Spain): Implications toward a revision of the middle Eocene biomagnetostratigraphy. Lethaia, 46, 293-307. DOI: https://doi.org/10.1111/let.12008

Tosquella, J., 1995. Els Nummulitinae del Paleocè-Eocè Inferior de la Conca Sudpirinenca. PhD Thesis. Barcelona, Universitat de Barcelona, unpublished, 581pp.

Tosquella, J., Serra-Kiel, J., 1998. Los Nummulítidos (Nummulites y Assilina) del Paleoceno Superior-Eoceno Inferior de la Cuenca Pirenaica: Sistemática. Acta Geologica Hispanica, 31(1-3), 37-159.

van der Voo, R., 1990. The reliability of paleomagnetic data. Tectonophysics, 184(1), 1-9.

Westerhold, T., Röhl, U., Frederichs, T., Agnini, C., Raffi, I., Zachos, J.C., Wilkens, R.H., 2017. Astronomical calibration of the Ypresian time scale: Implications for seafloor spreading rates and the chaotic behavior of the solar system? Climate of the Past, 13, 1129-1152.

Young, J.R., Bown, P.R., 1997. Proposals for a revised classification system for calcareous nannoplankton. Journal of Nannoplankton Research, 19(1), 15-47.

Zijderveld, J.D.A., 1967. AC Demagnetization of Rocks: Analysis of Results. In: Runcorn, S.K., Creer, K.M., Collinson, D.W. (eds.). Methods in Palaeomagnetism. Amsterdam, Elsevier, 254-286.

Manuscript received October 2021;
revision accepted May 2022;
published Online July 2022.